Inorganic Chemistry

pubs.acs.org/IC

Article

Does the Spin State and Oriented External Electric Field Boost the Efficiency of Fe(II) Pincer Catalyst toward CO_2 Hydrogenation Reaction?

Asmita Sen and Gopalan Rajaraman*

Cite This: *Inorg. Chem.* 2023, 62, 2342−2358

Read Online

ACCESS | Metrics & More | Article Recommendations | Supporting Information

ABSTRACT: In this study, we have explored the catalytic reactivities of four PNP-pincer supported Fe(II) complexes, namely, [(^{iPr}PN^{Me}P)-FeH$_2$(CO)] (**1**), [(^{iPr}PN^{Me}P)FeH(CO)(BH$_4$)] (**2**), [(^{iPr}PN^{H}P)-FeH$_2$(CO)] (**3**), and [(^{iPr}PN^{Me}P)FeH(BH$_4$)] (**4**) (^{iPr}PN^{Me}P = MeN-{CH$_2$CH$_2$(P^{i}Pr$_2$)}$_2$ and ^{iPr}PN^{H}P = HN{CH$_2$CH$_2$(P^{i}Pr$_2$)}$_2$) toward reductive CO_2 hydrogenation for formate production. Our density functional theory and ab initio complete active space self-consistent field study have identified three fundamental steps in this catalytic transformation: (i) anchoring of the CO_2 molecule in the vicinity of the metal using noncovalent interactions, (ii) catalyst regeneration via H_2 cleavage, and (iii) formate rebound step leading to catalytic poisoning. The variations in the catalytic efficiency observed among these catalysts were attributed to either easing of steps (i) and (ii) or the hampering step (iii). This can be achieved in various chemical/non-chemical ways, for instance, (a) incorporation of strong-field ligands such as CO facilitating single-state reactivity and eliminating two-state reactivity that generally enhances the rate and (b) inclusion of Lewis acids such as LiOTf and strong bases found to either avoid catalytic poisoning or ease the H−H cleavages, to enhance the rate of reaction (c) evading mixing of excited open-shell singlet states to the ground closed-shell singlet state that hampers the catalytic regeneration. We have probed the role of oriented external electric fields (OEEFs) in the entire mechanistic profile for the best and worst catalyst, and our study suggests that imposing OEEFs opposite to the reaction axis (z-axis) fastens the catalytic regeneration step and, at the same time, hampers catalytic poisoning. The application of OEEFs is found to regulate the energetics of various spin states and can hamper two-state reactivity, therefore increasing the efficiency. Thus, this study provides insights into the CO_2 hydrogenation mechanism where the role of bases/Lewis acid, ligand design, spin states, and electric field in a particular direction has been established and is, therefore, likely to pave the way forward for a new generation of catalysts.

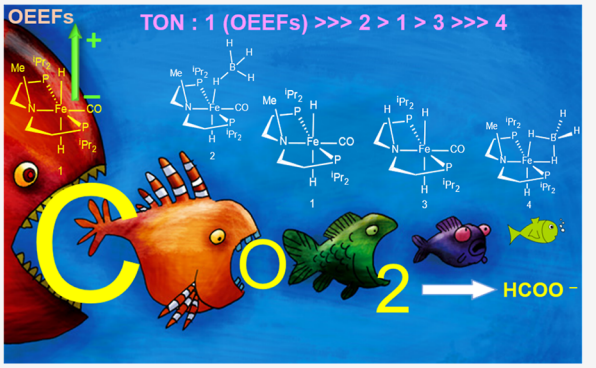

INTRODUCTION

Carbon dioxide (CO_2) is a well-known greenhouse gas, which is a non-toxic, abundant, and renewable carbon source present in the troposphere.[1] Continuous increase in the concentration of this gas in the atmospheric contributes to global warming, and chemical utilization of this widely spread, inexpensive C_1 source of carbon could mitigate climate change issues faced by humanity.[2−5] Therefore, many industrial approaches have been introduced in recent years to convert this chemical waste to value-added chemicals, and this procedure is known as carbon capture and utilization.[3,6,7] However, due to the very high inherent thermodynamic and kinetic stability of the C═O bonds in the carbon dioxide molecule, this renewable synthon always requires very rigorous reaction conditions and highly reactive catalysts to attain high yield and selectivity. These unfavorable conditions make the industrial processes for the utilization of CO_2 very tedious, expensive, and not practical. In the past few decades, significant efforts in this direction have been undertaken, and various catalysts based on transition metals have been synthesized for the utilization of CO_2.

CO_2-derived products are industrially synthesized in hazardous methods,[8,9] and because of the low atom economy of these traditional approaches, an alternative green route, where metal catalysts are being used for the direct introduction of the carbonyl group to the substrate, has become the area of attraction for the past few decades. Therefore, many experimental research groups are actively involved in the development of environmentally benign methods for the conversion of CO_2 to various feedstocks in the presence of molecular hydrogen (H_2).[10−14] In this direction, precious

Received: November 22, 2022
Published: January 23, 2023

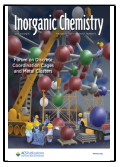

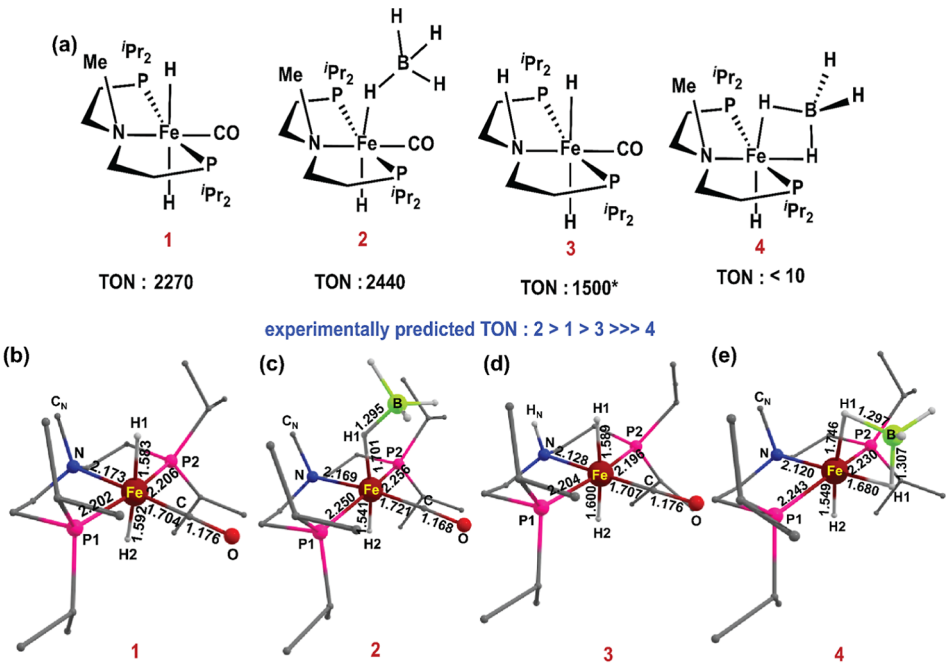

Figure 1. (a) Schematic geometry of the catalysts [(^{iPr}PN^{Me}P)FeH$_2$(CO)] (**1**), [(^{iPr}PN^{Me}P)FeH(CO)(BH$_4$)] (**2**), [(^{iPr}PN^{Me}P)FeH(CO)(BH$_4$)] (**3**), and [(^{iPr}PN^{Me}P)FeH(BH$_4$)] (**4**) with experimentally reported TONs, and density functional theory (DFT) optimized ground state geometries of (b−e) **1**−**4** along with selected structural parameters.

metals such as Ru, Rh, and Ir have been extensively employed in the past few decades for the production of formate, achieving turnover numbers (TON) and turnover frequencies of ∼3.5 × 10^6 and 150,000 h^{-1}, respectively,[15−21] indicating the remarkable potential of metal-based catalysts toward CO_2 activation. In 2015, a pincer-based noble metal complex, [(^{Ph}P^{Me}NP)RuClH(CO)], was reported as the most efficient catalyst for N-formylation reaction until now, achieving a TON of 1,850,000 toward the synthesis of 4-formylmorpholine.[22] Although these precious metal catalysts are proven to be highly effective, in recent times, concentration has been centered on the synthesis of the catalysts containing earth-abundant, low-cost, non-toxic base metals[23,24] such as Fe, Co, Mn, Ni, Cu, and Zn as the substitution of toxic noble metals (Ir, Ru, Rh), in expecting a greater economic and environmental advantage.[13] A series of PNP-pincer ligand-supported base metal-mediated catalysts reported to date are proven to be very effective in the activation and conversion of this highly stable species in a mild reaction condition with a satisfactory yield. Among them, the leading examples include a tetraphosphine-based Fe(II) catalyst and an ^{iPr}PN^{H}P-supported Co(II) chloride complex [(^{iPr}PN^{H}P)CoCl$_2$].[25,26] The former shows a better TON of 5100 as a pre-catalyst for the N-formylation of dimethyl and diethylamine, while the latter shows reactivity toward a large variety of primary and secondary amines with a TON of 130.

Recently, several PNP-pincer supported iron(II) carbonyl hydride catalysts, for instance, [(^{iPr}PN^{Me}P)FeH$_2$(CO)] (**1**), [(^{iPr}PN^{Me}P)FeH(CO)(BH$_4$)] (**2**), [(^{iPr}PN^{H}P)FeH(CO)(BH$_4$)] (**3**), and [(^{iPr}PN^{Me}P)FeH(BH$_4$)] (**4**) (Figure 1a) [where ^{iPr}PN^{Me}P = MeN{CH$_2$CH$_2$(P^{i}Pr$_2$)}$_2$ and ^{iPr}PN^{H}P = HN{CH$_2$CH$_2$(P^{i}Pr$_2$)}$_2$], have been reported and were proven to be excellent candidates for promoting the catalytic hydrogenation of CO_2 to formate and formamide. A TON as large as 2790 has been achieved with the 0.003 mol % of [(^{iPr}PN^{Me}P)FeH(CO) (BH$_4$)] catalyst forming formate salts in tetrahydrofuran (THF). This reaction was carried out under 69 atm pressure with a 1:1 CO_2/H_2 ratio at 80° in the presence of poor nucleophilic amine such as DBU (1,8-diazabicyclo[5.4.0]undec-7-ene). The TON is found to be largely enhanced and reached as high as ∼60,000 in the presence of the Lewis acid co-catalyst LiOTF.[13] This TON is the highest reported for any earth-abundant catalyst to date toward formate production. In a similar study by the same group, catalytic conditions for the N-formylation of morpholine by the same catalysts have been optimized, having a TON of 2440. It is shown that the [(^{iPr}PN^{Me}P)FeH(CO)(BH$_4$)] complex in the presence of excess amine rapidly eliminates BH_3 and forms a [(^{iPr}PN^{Me}P)FeH$_2$(CO)] complex, which also shows very similar activities for both formate formation and N-formylation reactions. In a structural analogous [(^{iPr}PN^{Me}P)-FeH(BH$_4$)] complex where the carbonyl group is absent, the catalytic activity is found to be drastically reduced with a TON of less than 10. These four catalysts with the TON varying from 10 to 2970 with small variations in their ligand architecture are intriguing examples to understand the role of ligand architecture in CO_2 sequestration.[11]

Several experimental and theoretical studies were devoted to understand the mechanism of CO_2 activation and to fine-tune the efficiency by varying the nature of the metal ions, ligand architecture, and various external additives such as Lewis acids and bases.[27−34] Besides the chemical ways to modify the efficiency of a catalyst, in recent times, an oriented external electric field (OEEF) has been suggested as a green co-catalyst to fine-tune important mechanistic steps in several reactions. For instance, it has been shown that a significant ionic character can arise in the homonuclear bonds such as H−H and Li−Li while applying OEEFs along the bond axis. It is argued that an X−Y type covalent bond can be viewed as the mixture of several resonance contributors like [X−Y ↔ X$^+$Y$^-$ ↔ XY$^+$].[35,36] In a certain electric field, these charged

https://doi.org/10.1021/acs.inorgchem.2c04119
Inorg. Chem. 2023, 62, 2342−2358

contributors are found to be stabilized, which in turn stabilizes a structure. Application of OEEFs in the high-valent Fe^{IV}=O-dependent porphyrin radical cation (CpdI) is found to regulate reactivity as well as regioselectivity of hydroxylation versus epoxidation during the reaction with propene as the substrate.[37] Moreover, the oxidative addition step in aryl halides (Ph−X) in a nucleophilic aromatic substitution CS_NAr process can be affected by the external electric field.[38] The tweezing effect of OEEFs is found to lower the reaction barrier of the halogen displacement reactions.[39] Therefore, the effect of external electric fields on the reactivity and product selectivity of a catalyst is wide ranging. Although the effect of OEEFs as an "invisible catalyst" has been explored in tuning the reactivity of various catalysts, its impact on the CO_2 activation reactions is unestablished.[40]

In this work, employing a combination of DFT and *ab initio* [complete active space self-consistent field (CASSCF)] calculations, we have explored the mechanism of formate production from CO_2 by complexes **1**−**4** with the aim to answer the following intriguing questions: (i) What are the important mechanistic steps in the reductive CO_2 hydrogenation to formate? (ii) Why do the TON numbers vary drastically from several thousand (**2**) to a few (**4**) with a slight alteration in the first coordination sphere? (iii) Is it possible to employ an OEEF as a non-chemical additive to enhance TONs?

COMPUTATIONAL DETAILS

All the DFT calculations were carried out using the Gaussian 16 (Revision C.01) suit.[41] The geometries of all stationary points were optimized without any restrictions using the dispersion corrected (D3) meta-generalized gradient approximation (GGA) M06-L density functional[42] in conjunction with a double-ξ quality LanL2DZ basis set with Los Alamos effective core potential[43] for the metal (Fe) and 6-31G(d) basis set for the rest of the atoms such as H, B, C, O, N, and P. The choice of the functional is based on the previous literature and related benchmarking available and the ability of the functional to account for noncovalent interactions. For instance, Truhlar and co-workers have shown that meta-GGA M06-L density functional successfully reproduces the ground state of most of the Fe(II)/Fe(III)/Fe(IV) species under investigation.[44] Ye and Neese groups have studied the CO_2 hydrogenation reactions catalyzed by $[M(H)(\eta^2\text{-}H_2)(PP_3^{Ph})]^{n+}$ (M = Fe(II), Ru(II), and Co(III); PP_3^{Ph} = tris(2-(diphenylphosphino)phenyl)phosphine)-type complexes employing the M06-L functional and have successfully established the rate-determining step which was in line with the experimental data.[27] We have performed a limited benchmarking to assess the spin state energy and their gap using various functionals and basis sets. This includes employing larger basis sets such as SDD (Fe) and 6-311G** (H, B, C, O, N, P) and all-electron basis sets such as TZVP in combination with other hybrid density functionals such as B3LYP-D3[45] and B3LYP*[46] with 15% of HF exchange and so forth (Table S1a). Calculations reveal that the ground S = 0 state remains unaltered with an energy gap of >170 kJ/mol between the ground state and high-spin (HS) state, offering confidence in the methodology chosen. The harmonic vibrational frequency calculations have been performed to characterize the nature of all stationary points. All global minima are identified by all positive frequencies, while the transition state is indicated by a single imaginary negative frequency. Intrinsic reaction coordinate calculations were performed at the same level to verify that the transition states connect the minima on either side of the saddle point. Dispersion correction to the optimized geometry and computed energetics is incorporated using the EmpiricalDispersion = GD3 keyword.[47] The energies were refined by the single-point calculations on the DFT optimized structures at the same level of theory using an all-electron Def2-TZVPP basis set.[48] The effect of solvation has been incorporated by employing the SMD solvation model[49] using THF as a solvent. Therefore, the final energies are the solvation and zero-point energy corrected higher-level electronic energies. To assess and analyze the stability of the wavefunction computed in DFT calculations, we have performed additional stability check using the stable = opt keyword in G16. All the species and their energies reported here are obtained from a stable wavefunction tested under this condition.

The effect of a finite electric field has been incorporated into the calculations using the "field = $M \pm N$" keyword available in Gaussian 16. The notation defines the axis of OEEF (M) and its direction ($\pm$) and magnitude (N) in au. The strength of the electric field has varied between $F = -4.5 \times 10^{-3}$ au and $F = +4.5 \times 10^{-3}$ au (where 1 au = 51.4 V/Å). The electric field is oriented along the Z-axis, which is the Fe−H bond direction from where the CO_2 approaches and interacts with the catalyst. Other than the chosen Z-axis, it is also possible to apply the electric field in other directions, such as that along the Fe−CO bond, which can either enhance the crystal field if the Fe−CO bond shortens or weaken the crystal field if the Fe−CO bond elongates. The weakening of the crystal field is expected to worsen the catalytic efficiency because this is expected to bring the excited state closer to the ground state (vide infra).

At first, complete geometry optimization of various reactants, intermediates, and transition states was performed using the same level of theory in the presence of an electric field of various strengths. This results in the evaluation of geometrical changes in the presence of OEEFs. Further, to account for the variation in energy on the optimized geometries, single-point calculations have been performed in the presence of OEEFs. Similar to the field-free methods, the effect of solvation on the net energy has also been explored with THF using the SMD solvation model with the UM06-L/Def2-TZVPP methodology. Here, simultaneous use of solvation and electric fields may lead to a variety of issues related to solvent dynamics; nevertheless, since the applied field is of moderate range in a non-polar solvent, this problem should be less relevant.

The natural bonding orbital (NBO) and deformation energy analysis have been performed using the Gaussian 16 suit of program. To ascertain the nature of the oxidation state of the metal ion during the course of the reaction, natural population analysis (NPA) charges were computed for catalyst **1** for all species in the potential energy surface, and it was found to vary only by ∼0.25 across all species, suggesting that the oxidation state is maintained. The deformation energy (ΔE_{def})[50−52] has been calculated to obtain the destabilizing steric energy associated with the transition states, which is known to be the main factor behind the energy barrier. The transition states are divided into two fragments: A (catalyst part) and B (substrate part). The solvent phase single-point calculation, as well as frequency calculations, has been performed on them. Then, the summation of these two energies was subtracted from the summation of energies of the free catalyst and

https://doi.org/10.1021/acs.inorgchem.2c04119
Inorg. Chem. 2023, 62, 2342−2358

Scheme 1. Regeneration of 2 to 1 and the Participation of 1 in the CO_2 Hydrogenation Reaction to Produce Formate ($HCOO^-$) Followed by the Regeneration of 1 in the Absence/Presence of BH_3

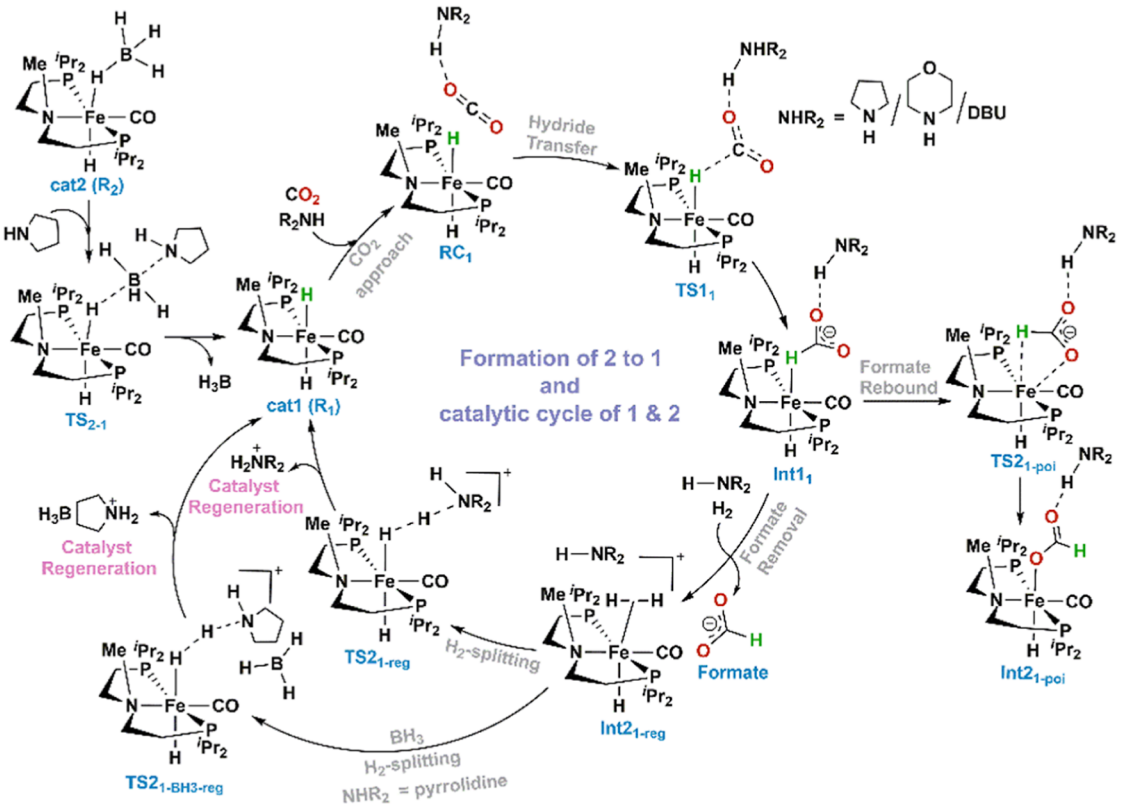

substrate ($E_{solvation}$ + ZPC). While the deformation energy reflects the amount of strain present in the geometries at the transition state, there are cases where H···H bond cleavage has also been incorporated due to the nature of fragments chosen (e.g., as in the case of $TS2_{reg}$).

Therefore,

$$\Delta E_{def} = TS(A + B)(E_{solvation} + ZPC) - A(E_{solvation} + ZPC) - B(E_{solvation} + ZPC)$$

All ab initio single-point calculations have been performed on the DFT-optimized geometries of the intermediates and the transition states using the ORCA 4.2.1 program.[53] The Douglas−Kroll−Hess (DKH) Hamiltonian has been employed to account for the scaler relativistic effect. During the calculations, the DKH-contracted version of the basis sets was used—DKH-def2-TZVP for Fe, DKH-def2-TZVP(-f) for directly coordinated atoms (N, P, C, H in **1**−**3** and N, P, H in cat **4**) to the metal, and DKH-def2-SVP for the rest of the atoms which are not directly connected to the metal.[54] We have also tested the role of the relativistic effect by performing additional calculations using ZORA, and the results obtained from these tests are very similar to those obtained from DKH methods. The calculations performed excluding any relativistic effects yielded slightly different percent contributions but have not dramatically altered the overall trend. In the next orbital-optimization step, the state-averaged CASSCF (SA-CASSCF)[55] calculations have been performed using the same basis set. A CASSCF calculation including six metal electrons distributed in 5 metal d-orbitals with 5 quintet, 45 triplet, and 50 singlets roots have been considered. We have also performed additional calculations using extended reference space, a CAS(8,6) calculation, wherein the hydride atom and its electrons were incorporated in the reference space along with 5d orbitals. While this extended reference space was found to alter the per cent contribution, the minor-major component, as well as the trend, remained unaltered. These additional benchmarking results are given in Table S1a. As the exact percent contribution is subject to variation with respect to the active space and basis set, we have focused mostly on the trend among different species that remain similar. All stationary points were denoted as $^{(2S+1)}Y_X$. Here, *Y* is *RC* for the reactant complex, *INT* for intermediates, and *TS* for transition states, and X denotes the catalysts **1**−**4** employed. The overall spin multiplicity is mentioned as a superscript on the extreme left to the general description as (2S + 1). This is mentioned for all spin states except for the S = 0 spin state corresponding to the catalysts **1**−**4**.

RESULTS

Spin-State Energetics of 1−4. The ground state optimized structures of **1**−**4** are shown in Figure 1b. While **1** contains an $^{iPr}PN^{Me}P$ pincer type ligand along with two hydrides in a trans-position, and one carbonyl, the Fe(II) center in **2**, has a $[BH_4]^-$ unit in a cis-position to the tertiary amine group and trans to another hydride. In **3**, a secondary amine group ($^{iPr}PN^{H}P$) is utilized to investigate the role of the methyl group attached to the amine in the PNP ligand. In **4**, the equatorial CO ligand is absent so that the role of a stronger π-acceptor ligand and spin state could be explored. DFT calculations yield an S = 0 spin state as the ground state for all four catalysts **1**−**4** with the S = 2 high-spin (HS) and the S = 1 intermediate-spin (IS) states lying above 84.0 kJ/mol for **1**−**3**. A very large energy gap between the ground state (S = 0) and

https://doi.org/10.1021/acs.inorgchem.2c04119
Inorg. Chem. 2023, 62, 2342−2358

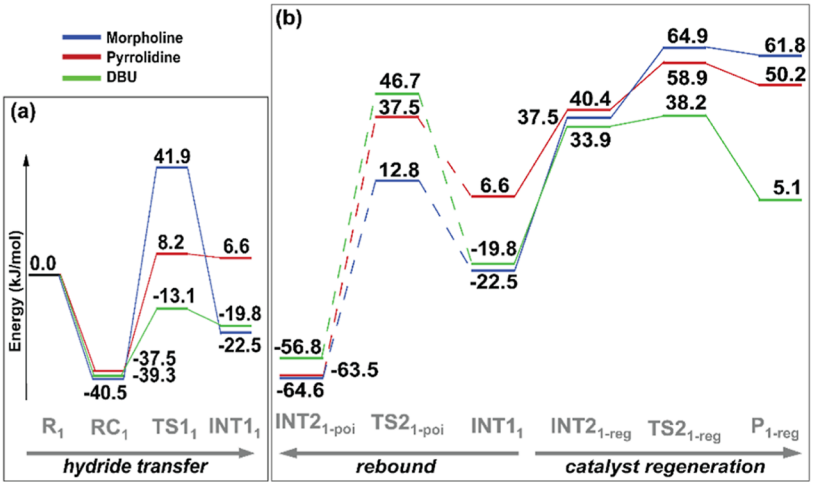

Figure 2. DFT computed energy profile diagram (kJ/mol) for (a) the hydride transfer followed by the (b) catalyst regeneration vs the formate rebound pathway in catalytic hydrogenation of CO_2 by **1**.

the high-lying HS/IS states is indicative that these spin states are unlikely to participate in the reaction mechanism, eliminating the possibility of two-state/multistate (TSR/MSR) reactivity for these catalysts. This is affirmed by the potential energy surface computed where all the transition states and intermediates at the S = 0 surface were found to be lower than the ballpark number of 84 kJ/mol (vide infra). For **4**, on the other hand, S = 2 and S = 1 states are close lying, that is, at 34.5 and 19.2 kJ/mol, respectively, from the ground state, suggesting a possibility for the observation of TSR/MSR reactivity. The S = 0 ground state observed in **4** indicates that BH_4^- also is a strong field ligand, though the strength of the ligand field is relatively weaker compared to the CO ligand leading to close-lying S = 2 and S = 1 states.

Mechanism of Base-Assisted Hydrogenation of CO_2. The reductive hydrogenation of CO_2 resulting in the formation of formate salt ($HCOO^-$) takes place in four fundamental steps: (i) approach of the CO_2 molecule toward the catalyst, leading to the formation of the reactant complex (*RC* [LFe(H)(X)[CO_2]); (ii) transfer of the hydride from the metal center to the electronically deficient CO_2, leading to the hydrogen-bound formate intermediate (*INT1* [LFe···H−COO]) via *TS1*; (iii) base-assisted release of formate followed by the activation of dihydrogen ($INT2_{reg}$ [LFe−H_2]); and finally, (iv) regeneration of the metal-hydride species (*R*, [LFe(H)]) via heterolytic H−H cleavage in the presence of a base (Scheme 1) via $TS2_{reg}$. Alternatively, after forming the hydrogen-bound formate intermediate (*INT1*) species, the reaction can diverge to oxygen-bound formate intermediate LFe···O−COH ($INT2_{poi}$) via the formate rebound transition state $TS2_{poi}$. The formation of $INT2_{poi}$ can be considered catalytic poisoning as the Fe−O(formate) bond is expected to be very stable, rendering the removal of formate, resulting in an energy-demanding process. Therefore, the catalyst is unlikely to be regenerated, reducing the catalytic efficiency. To untangle the response of various stationary points (intermediates and transition states) in the presence of bases with different pK_a values and steric crowding, we have studied CO_2 to formate production energetics in the presence of three bases: pyrrolidine (pK_a = 11.27), morpholine (pK_a = 8.51), and DBU (pK_a = 24.34).[56,57]

Computed energetics (Figure 2, Table S1b) reveal that the formation of *RC* is exothermic in the presence of pyrrolidine by −37.5 kJ/mol (−40.5 and −39.3 kJ/mol for morpholine and DBU), indicating that the interaction of the catalyst with CO_2 and bases is favorable. A closer look at the *RC* (Figure 3a) suggests strong ($^i pr_2$)C−H···O(CO) interactions between the isopropyl groups of PNP-pincer ligand, and the CO_2 (2.505 and 2.583; 2.502 and 2.564; 2.438 and 2.601 Å for pyrrolidine, morpholine, and DBU, respectively) molecule along with a (*Pyrr*)N−H···O(CO) interaction (2.478 and 2.605 Å for pyrrolidine and morpholine respectively, Figures S1, 3a) helps to anchor the CO_2 to the catalyst in this step. Further, we detected a weak interaction between the electron-deficient carbon atom of the CO_2 and hydride H atom with an (Fe)H···C(O_2) distance of 2.796 Å (2.789 and 2.952 Å in morpholine and DBU, respectively), which is also reflected in the computed charges, suggesting partial activation of CO_2 at this stage.

In the next step, this hydride gets transferred to the CO_2 forming *INT1*, which is found to be slightly endothermic in the presence of pyrrolidine by 6.6 kJ/mol with a barrier of 45.7 kJ/mol from the respective *RC* (−22.5 and 82.4 kJ/mol for morpholine and −19.8 and 26.2 kJ/mol for DBU, respectively). In $TS1_{1\text{-}pyrr}$, the Fe−H bond is elongated to 1.718 Å (1.699 and 1.640 Å, respectively, for $TS1_{1\text{-}mor}$ and $TS1_{1\text{-}DBU}$) with H···C(O_2) distance shortening to 1.535 Å (1.555 and 1.596 Å, respectively, for $TS1_{1\text{-}mor}$ and $TS1_{1\text{-}DBU}$; Figure S2). The nature of this transition state is product-like for pyrroline, while it is reactant-like for DBU, rationalizing the relatively lower barrier observed with the latter. In $INT1_{1\text{-}pyrr}$, the Fe−H bond is further elongated by 0.125 Å (0.136 and 0.077 Å, respectively, for $INT1_{1\text{-}mor}$ and $INT1_{1\text{-}DBU}$) in addition to the formation of a new H−C bond of 1.272 Å (1.268 and 1.276 Å, respectively, for $INT1_{1\text{-}DBU}$ and $INT1_{1\text{-}mor}$; Figure S3) between the hydride and the electron-deficient C-atom in CO_2. In $INT1_{1\text{-}pyrr}$, although the hydride is transferred to C_{CO_2}, a frail interaction between the Fe and the hydride is still present. Also, at this intermediate, the (*Pyrr*)N−H···O(CO) interaction is very strong (2.223 Å), aiding the removal of formate ion, forming an unstable penta-coordinated mono-cationic Fe(II) species which upon reaction with H_2 gas forms $INT2_{reg}$ [LFe−H_2]$^+$ (Figure S4). The formation of the [LFe−H_2]$^+$ species is found to be endothermic by 37.5, 40.4, and 33.9 kJ/mol from the free catalyst in pyrrolidine, morpholine, and DBU,

https://doi.org/10.1021/acs.inorgchem.2c04119
Inorg. Chem. 2023, 62, 2342−2358

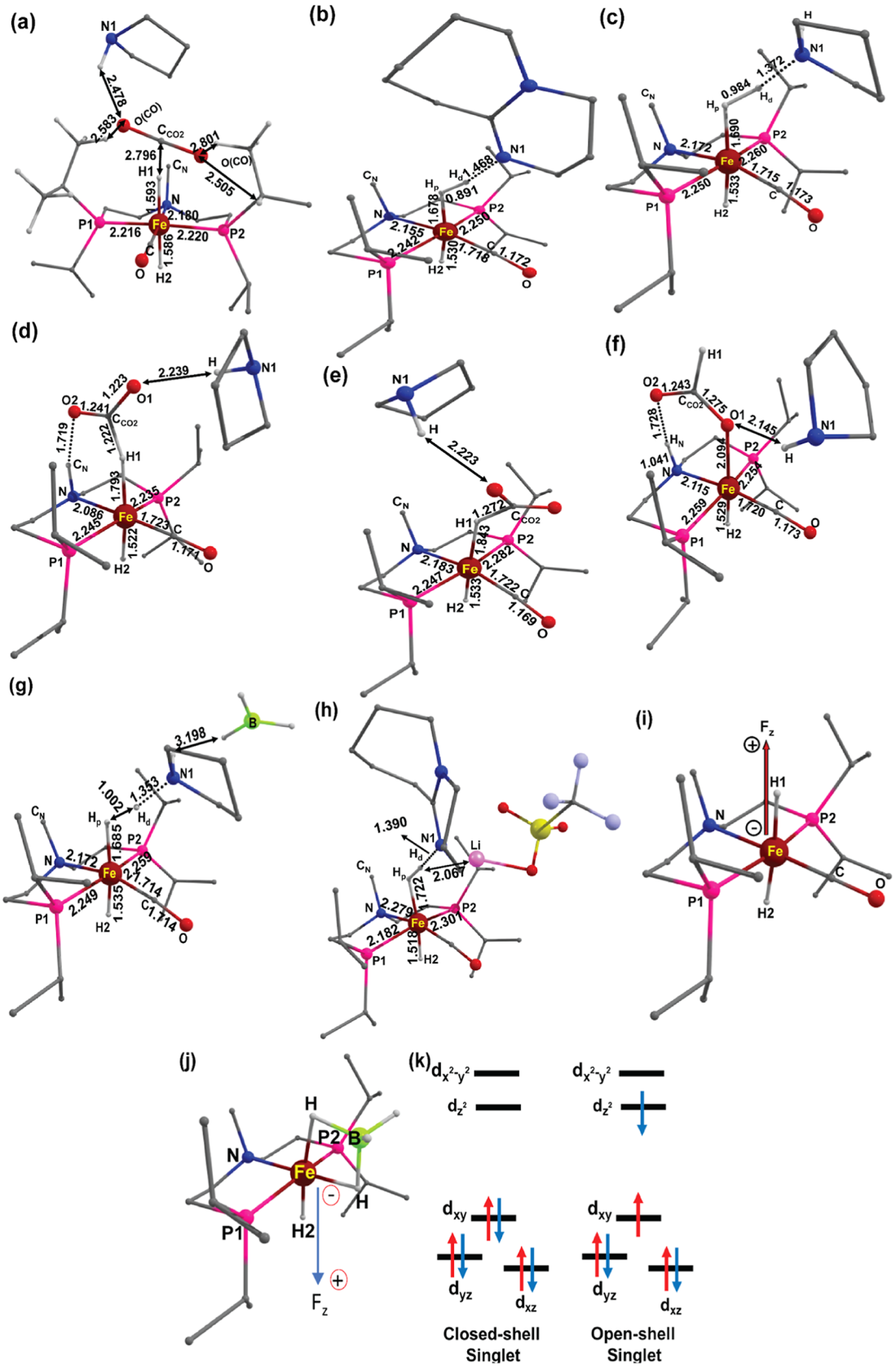

Figure 3. DFT optimized ground state geometries of (a) $RC_{1\text{-pyrr}}$, (b) $TS2_{1\text{-reg-DBU}}$, (c) $TS2_{1\text{-reg-pyrr}}$, (d) $INT1_3$, (e) $INT1_{1\text{-pyrr}}$, (f) $INT2_{3\text{-poi-pyrr}}$, (g) $TS2_{1\text{-reg-BH3}}$, (h) $TS2_{1\text{-reg-LiOTf}}$, (i,j) definitions of the *z*-directions, along with the definitions of a positive OEEF ($F_z > 0$) Gaussian 16 in **1** and **4**, and (k) closed-shell vs open-shell singlet configuration.

https://doi.org/10.1021/acs.inorgchem.2c04119
Inorg. Chem. 2023, 62, 2342−2358

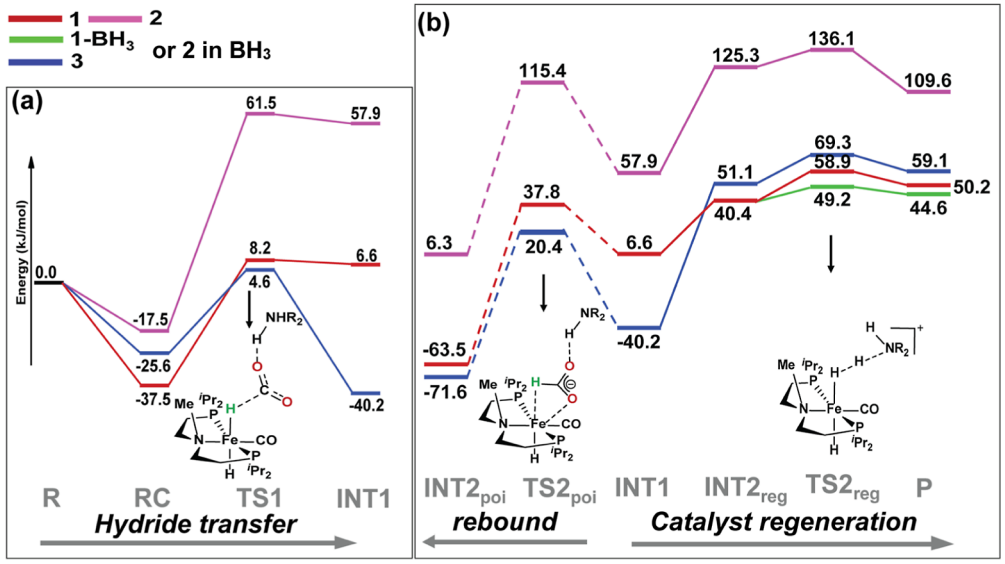

Figure 4. DFT computed energy profile diagram (kJ/mol) for (a) the hydride transfer followed by the (b) catalyst regeneration vs formate rebound pathway in catalytic hydrogenation of CO_2 by **1**−**3**.

respectively. In the next step, catalytic regeneration assisted by the base is assumed to take place via $TS2_{reg}$, which is found to have a barrier of 58.9, 64.9, and 38.2 kJ/mol for pyrrolidine, morpholine, and DBU bases, respectively. This step is estimated to be the rate-limiting step, and therefore, the differences in the estimated barrier heights are correlated to the rate of the reaction and hence the associated TONs. As the DBU is the strongest base among the three, the barrier is substantially smaller. To understand the steric contribution to the rate-limiting transition state, we have calculated the deformation energy of the corresponding step, which is found to be 127.9, 129.9, and 100.4 kJ/mol in the presence of pyrrolidine, morpholine, and DBU, respectively. Lower deformation energy and hence the barrier height found for DBU are associated with the fact that the corresponding $TS2_{1\text{-}reg\text{-}DBU}$ (Figure 3b) is more reactive compared to $TS2_{1\text{-}reg\text{-}pyrr}$ (Figure 3c) and $TS2_{1\text{-}reg\text{-}mor}$. The strongest basic character of DBU facilitates proton abstraction even with a longer N···H distance (1.468 Å) which is not possible with the other two bases (1.372 and 1.336 Å for pyrrolidine and morpholine, respectively, Figure S5). In other words, the morpholine and pyrrolidine approach closer to the hydrogen atom at the transition state creates a significant steric strain.

The catalytic poisoning step is found to be highly exothermic in nature, with −63.5, −64.6, and −56.8 kJ/mol for pyrrolidine, morpholine, and DBU, respectively, due to the formation of a favorable Fe−O bond. The kinetic requirement for the formation of $INT2_{poi}$ (Figure S6) is estimated to be 12.8, 37.5, and 46.7 kJ/mol ($R_1 \rightarrow TS2_{1\text{-}poi}$, Figure S7) in the presence of morpholine, pyrrolidine, and DBU, respectively. This energy penalty is also in line with the calculated deformation energies in these species (84.8, 86.3, and 94.3 kJ/mol). For DBU, the barrier is much larger as the steric strain is higher, suggesting the unfavorable formation of this catalytic poison step among the three bases discussed. The cleavage of formate from $INT2_{poi}$ is found to be exceedingly endothermic (>200 kJ/mol), suggesting that the catalytic poisoning step is not favorable for this catalyst. To understand the kinetic requirements for the Fe−O bond cleavage in $INT2_{poi}$ versus Fe−H bond cleavage in *INT1*, we have performed relaxed potential energy scans along the Fe−O and Fe−H bonds (Fe−O {Fe−H bond lengths varied from 2.023{1.843} to 3.166 {3.243} Å), respectively (Figure S8). As we elongate the Fe−H bond, the energy increases until 2.543 Å, reaching ∼78.0 kJ/mol, suggesting a favorable reaction beyond which the energy drops. For the Fe−O bond, on the other hand, the energy penalty of elongating the Fe−O bond exceeds 100 kJ/mol at 3.125 Å, beyond which, due to the bidentate character of formate, the other oxygen is found to bind with Fe, leading to a monotonous increase of energy. This suggests that the Fe−O bond is rather hard to cleave without external stimuli.

Catalyst **3** (Scheme S1) also follows the same mechanistic pathway as **2** (Figures S9−S12). The $INT1_3$ formations estimated to be highly exothermic. This is attributed to a strong intramolecular hydrogen bonding interaction between one of the oxygen atoms of the formate and the hydrogen atom of the secondary amine group in the PN^HP pincer (1.719 Å). This PNP(H)···O(HCO) interaction results in the formation of a highly stable six-membered ring, which facilitates the formation of $INT1_3$ with a lower energy penalty (Figure 3d). In catalyst **1**, on the other hand, there is no scope for intramolecular hydrogen bonding, and hence, it was comparatively uphill by 44.1 kJ/mol from *RC* (Figure 3e). This stability due to H-bonding interaction remains intact in $INT2_{3\text{-}poi}$ (Figure 3f). Because of this, the formation of $INT2_{3\text{-}poi}$ is exceedingly exothermic (−71.6 kJ/mol) among all species studied here. Further, the conversion of $INT1_3$ to $INT2_{3\text{-}poi}$ has a very low kinetic requirement (20.4 kJ/mol) via $TS2_{3\text{-}poi}$. The O···C bond of the formate involved in intramolecular H-bonding interaction was found to be longer in **3** compared to **2** (1.241 vs 1.223 Å), which enables relatively free rotation, leading to the lowest rebound barrier. In $TS2_{3\text{-}poi}$, the limiting values of breaking Fe−H and forming Fe−O are found to be 2.130 and 2.682 Å, while the oxygen end is in close contact (2.030 Å) with the secondary hydrogen of amine (Figure S12). This Fe−O bond is completely formed (2.094 Å) in $INT2_{3\text{-}poi}$, and the Fe−O oxygen remains hydrogen bonded (1.728 Å) (Figures 3f and S13). Thus, the N−H moiety was found to significantly influence catalytic poisoning,

https://doi.org/10.1021/acs.inorgchem.2c04119
Inorg. Chem. 2023, 62, 2342−2358

leading to faster poisoning by catalyst **3** than **2**. Further, the regular catalytic regeneration is found to be exceedingly endothermic by 91.3 kJ/mol ($INT1_3$ to $INT2_{3\text{-}reg}$, the highest among all catalysts; Figure 4, blue graph). The steps in the catalytic regeneration were also found to have an energy penalty (18.2 kJ/mol for $INT2_{3\text{-}reg} \rightarrow TS2_{3\text{-}reg}$; Figure S14), suggesting that catalytic regeneration in **3** has a steep energy penalty diminishing TONs. A part of this energy penalty stems from intramolecular hydrogen bonding PNP(H)···O(HCO) interaction which needs to be ruptured to yield a product, adding additional energy costs. This drastically reduces the TON as observed in the experiments.

Effect of Lewis Acids. Experimental results suggest that **2** acts as a pre-catalyst which, in the presence of an excess base (here we are taking pyrrolidine as a base), rapidly removes the BH_3 unit forming the active catalyst **1** (Scheme 1). The DFT computed intrinsic barrier for the removal of BH_3 forming active species **1** is estimated to be 56.8 kJ/mol (conversion of **2** to **1** via $TS_{2\text{-}1}$). This barrier is relatively smaller than other steps discussed for **1**, and the conversion is also exothermic by 29.2 kJ/mol, easing the energy penalty further. After the conversion of **2** to **1**, the pathway for CO_2 activation is the same for both. Experimentally, the TON measured for **2** is higher than that for **1** (2440 vs 2270 in morpholine),[57] and this mechanistic proposal does not explain this observation. The catalyst **2**, upon conversion to **1**, also generates the BH_3 molecule, and therefore, we explored the possible role of this Lewis acid in the rate-determining step, that is, catalytic regeneration. A combination of pyrroline and BH_3 leads to a quaternary adduct which is expected to aid the H−H cleavage via $TS2_{1\text{-}BH3\text{-}reg}$ (Figure 3g), and this is found to have a barrier of 49.2 kJ/mol compared to 58.4 kJ/mol found in the absence of BH_3 (Figure 4, green line). This lower barrier in the rate-limiting step, along with the exothermic conversion of **1** to **2**, results in a larger TON for **2**. Although there is a barrier to the transformation of **2** to **1**, this is a one-time energy penalty and therefore does not hinder the TON. Even though the rate-determining barrier is decreased only by ∼9 kJ/mol in the presence of BH_3, this step is part of the catalytic cycle that dictates the TON. Therefore, any reduction, however small, facilitates a larger TON.

The experiment suggests that the reaction TON of **1** and **2** enhanced drastically in the presence of Lewis acid and LiOTf and reached as high as ∼60,000. To understand this process, we have modeled the CO_2 hydrogenation of **1** in the presence of Lewis acid LiOTf. Calculations reveal that the formation of *RC* is highly exothermic in nature RC_{LiOTf} (−288.7 kJ/mol, Figure S15). The very high exothermicity is attributed to several ionic as well as noncovalent C−H···N(O) interactions between the cationic/anionic part of the Lewis acids, catalysts, and DBU. Unexpectedly, the formate rebound mechanism leading to catalyst poison product ($INT2_{poi}$) via $TS2_{poi}$ is found to be very less energy demanding (<28 kJ/mol). This is contradictory to the very high TON in the presence of external stimuli like Lewis acid. Therefore, we have calculated the energy required to break the Fe−O bond in $INT2_{poi}$ in the presence of these chemical stimuli. Li ion is found to facilitate the Fe−O bond cleavage from $INT2_{poi}$ with a very less energy penalty (<25 kJ/mol) in all cases, and therefore, the catalyst is regenerated from the catalytic poisoning (Figure S16). This enhances the TON significantly as there is no catalytic poisoning in the presence of such salts. The H−H bond cleavage is found to be highly energy demanding for $TS2_{reg\text{-}LiOTf}$ (100.4 kJ/mol; Figure 3h). In the presence of LiOTf as an external stimulus, although the energy barrier for the H···H bond cleavage is not smaller, it can be fully compensated by the exothermicity of the *RC* formation. The $TS2_{reg\text{-}LiOTf}$ transition state lies at −195.9 kJ/mol, followed by the formation of the product, which is at −257.7 kJ/mol. Therefore, per catalytic cycle, the energetic gain will be −188.3 kJ/mol ($RC_{LiOTf} - TS2_{reg\text{-}LiOTf}$), which will be carried to the next cycle. This is in line with the highest obtained TON in the presence of LiOTf in DBU.

Mimicking the Role of External Additives Using OEEF by 1. In the chemical approach, different bases and Lewis acids have been employed to attain catalytic efficiency toward CO_2 activation. Our DFT calculations have shown that external stimuli lower the barrier for catalytic regeneration and augment the barrier for the formate rebound. For instance, the strongest base DBU reduces the intrinsic barrier for the catalyst regeneration and, at the same time, hinders the formate rebound step, resulting in greater efficiency. From this mechanistic perspective, it clearly emerges that an external additive is required whose basicity should be so high that it can cleave dihydrogen from a long distance to avoid energy penalty due to steric crowding. However, finding a perfect additive which is highly basic as well as results in less steric effect is challenging and requires a rigorous optimization process. In this direction, we have explored an alternative approach to enhance the efficiency of these catalytic reactions using an OEEF as a green additive.[35,37−39,58]

An external electric field ranging from $\pm 0.1 \times 10^{-3}$ au to $\pm 4.5 \times 10^{-3}$ au has been applied by orienting it along the Fe−H1 axis (*z*-axis, Figure 3i). From the energy profile diagram depicted in Figure 5, it is seen that the electric field oriented along both the +*z*-axis (H2−Fe−H1 direction) and the −*z*-axis (H1−Fe−H2 direction) stabilizes the *RC* compared to the field-free condition. However, the stability of *RC* is much greater for the +*z*-direction (energy margin of 30.3 kJ/mol with the highest OEEF value of 4.5×10^{-3}) compared to the −*z*-direction (energy margin of 8.3 kJ/mol with highest OEEF value of -4.5×10^{-3}; Figure 5a). In the +*z*-direction, the H2−Fe distances become shorter and Fe−H1 distances become longer with increasing field strength (by ∼0.011 Å; Table S2), while a reverse scenario is noted for the −*z*-direction. An increase in the Fe−H1 distance along the positive *z*-direction was also found to diminish the H1···C(O2) distance, leading to greater interaction with CO_2 and larger stability. Moreover, the CO_2 was found to be also better anchored with stronger noncovalent interactions to the catalyst by applying an electric field in the +*z*-direction ((*Pyrr*)N−H···O(CO): 2.461 Å and ($^i pr_2$)C−H···O(CO): 2.544, 2.591, 2.519, 2.766 Å in 4.5×10^{-3} au), and the reverse was noted while applying a field in the −*z*-direction, regenerating a weaker noncovalent interaction ((*Pyrr*)N−H···O(CO): 2.534 Å and ($^i pr_2$)C−H···O(CO): 2.561, 2.633, 2.486, 2.851 Å in 4.5×10^{-3} au). All these factors are directly correlated to the higher stability along the H2−Fe−H1 direction.

Similarly, the hydride transfer transition ($TS1_1$) state is stabilized (as high as 20.7 kJ/mol), yielding lower barriers along the +*z*-direction if the field strength varies from 0.1×10^{-3} to 4.5×10^{-3} au. The same transition state gets destabilized in the −*z*-direction (as much as 31.4 kJ/mol). This alters the corresponding kinetic requirement; for example, at the highest field value applied along the +*z*-direction, the barrier is 24.9 versus 45.7 kJ/mol in field-free conditions.

https://doi.org/10.1021/acs.inorgchem.2c04119
Inorg. Chem. 2023, 62, 2342−2358

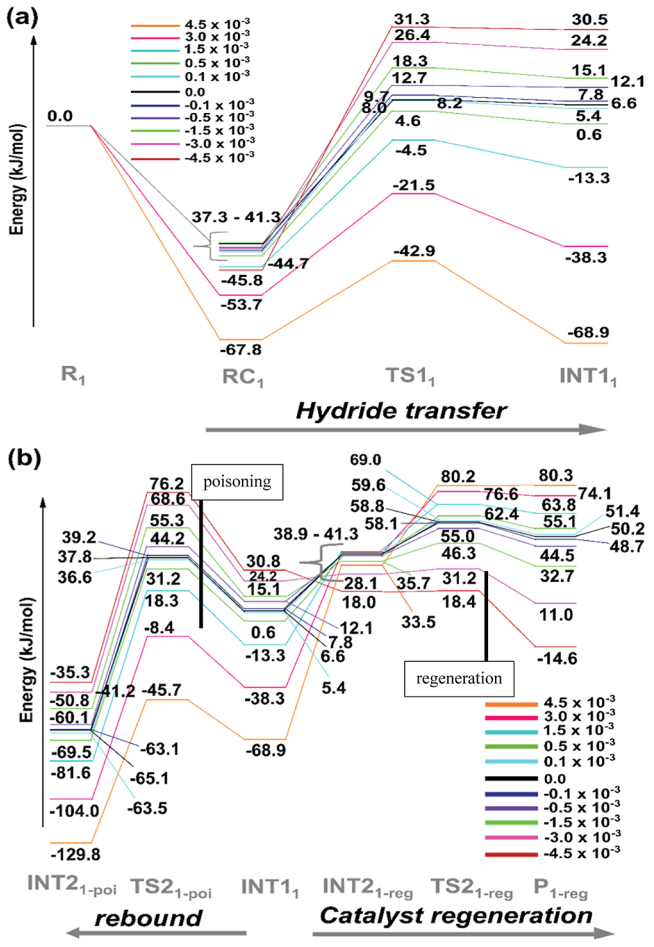

Figure 5. DFT computed energy profile diagram (kJ/mol) for (a) the hydride transfer followed by the (b) catalyst regeneration vs the formate rebound pathway in catalytic hydrogenation of CO_2 by **1** in different magnitudes of OEEF.

However, along the −*z*-direction, the barrier is enhanced to 77.1 kJ/mol, though from the free reactant, the barrier is only 31.4 kJ/mol. Careful investigation of the transition state structure during hydride transfer reveals that increasing the field strength in the +*z*-direction increases the polarity of the Fe−H1 bond along with a gradual increase of negative charge on the hydride H1 atom (−0.050 vs −0.080 in the field-free vs 4.5×10^{-3} au field), enabling the hydride attack from a larger (Fe)H···C(O2) distance, reducing the intrinsic energy barrier (Table S3). A reverse scenario is noted if we apply an electric field in the −*z*-direction. A similar trend is also observed in *INT1*, whose exothermicity increases along the +*z*-direction by a margin of 75.5 kJ/mol. The formation of *INT1* is endothermic in the −*z*-direction, leading to +27.2 kJ/mol of endothermicity at -4.5×10^{-3} au OEEF. While the formation of $INT2_{reg}$ is mostly isothermal with respect to the field-free state (40.4 kJ/mol) in the presence of an electric field in the +*z*-direction, the stability of this intermediate increases gradually with the application of OEEF in the −*z*-direction. The intrinsic barrier for the heterogeneous H_2 cleavage was found to increase from 58.8 kJ/mol in the field-free state to 80.2 kJ/mol in the presence of an electric field of $+4.5 \times 10^{-3}$ au. For the −*z*-direction, the energy barrier diminishes significantly and reaches as low as 18.4 kJ/mol at the highest value of OEEF applied. A careful analysis of the geometry reveals that in the +*z*-direction, the $H_p \cdots H_d$ (here subscript p and d denote proximal and distal positions with respect to Fe) distance increases (∼0.15 Å at $+4.5 \times 10^{-3}$ au) with an increase in the applied field strength, and this, in turn, brings the base closer to the H_d (shorter $H_d \cdots N(Pyrr)$ distance; Table S3), enhancing the steric strain and resulting in a larger barrier. For the −*z*-direction, on the other hand, the $H_p \cdots H_d$ distances shorten by ∼0.08 Å (-4.5×10^{-3} au), which in turn keeps the base away, reducing the strain and resulting in a lower barrier. The computed NBO charges also support the idea that at a shorter $H_p \cdots H_d$ distance, the charge on the N(*Pyrr*) is larger (−0.679 vs −0.689 in the field free vs -4.5×10^{-3} au). Hence, electrostatic interactions are favorable even at a larger distance for proton abstraction (Table S4), facilitating the H−H cleavage.

Alternatively, a formate rebound can occur from *INT1*, forming $INT2_{poi}$, which is proposed to be a catalytic poison step in this study, found to show a contrasting behavior in the presence of an electric field as compared to its competitive counterpart, that is, the catalyst regeneration pathway. While an electric field in the −*z*-direction favors the catalyst regeneration process by drastically reducing the heterogeneous H_2-cleavage barrier, the same amount of OEEF in the same direction considerably increases the formate rebound energetic cost as high as 76.2 kJ/mol at -4.5×10^{-3} au field. As expected, an electric field in the +*z*-direction results in the reduction of the formate rebound energy barrier to merely 23.2 kJ/mol from the respective *INT1*, facilitating faster catalytic poisoning. With an electric field operation through the H2−Fe direction (+*z*-direction), the natural charges on the metal center decrease gradually, from −1.138 in the field-free state to −1.086 at 4.5×10^{-3} au field, with an accumulation of negative charge on the oxygen atom (−0.705 in the field-free state to −0.724 in -4.5×10^{-3} au field; Table S4) which is involved in the rebound process. This increase in charge separation between two centers involved in bond formation facilitates the formate rebound. In the −*z*-direction, on the other hand, the charge on the rebound oxygen remains unaltered (−0.706 in -4.5×10^{-3} au field) and the charge on Fe is slightly decreases (reaches −1.125 in -4.5×10^{-3} au field), making the rebound step unfavorable. Therefore, in an electric field of -4.5×10^{-3} au, catalytic poisoning is expected to be quenched significantly, leading to a tremendous increase in the reaction TONs. In the absence of an electric field, the heterogeneous H_2-cleavage forming a regenerated catalyst step is identified as the rate-limiting step, while the application of OEEF in the −*z*-direction reduces this barrier to 18.4 kJ/mol at 4.5×10^{-3} au, revealing that this step is no longer rate determining. In the same condition, the energy requirement for the hydride transfer was found to be increased to 77.1 kJ/mol from the respective *RC* species (4.5×10^{-3} au along the H1−Fe−H2 axis). Therefore, at the 4.5×10^{-3} au electric field in the −*z*-direction, the hydride transfer step becomes the rate-determining one, and the energy penalty of 31.3 kJ/mol is compensated by the energy gain of 40.4 kJ/mol during the catalyst regeneration as compared to the field-free state (Figure 5b). The computed deformation energy suggests that in $TS2_{reg}$ along the +*z*-direction, the higher barrier for catalyst regeneration is contributed by the steric contributions (Table S5). While experimental proof for this prediction is not available yet, it is important to note here that LiOTf, when used, increases the TON by 60,000, and this is likely to play a

https://doi.org/10.1021/acs.inorgchem.2c04119
Inorg. Chem. 2023, 62, 2342−2358

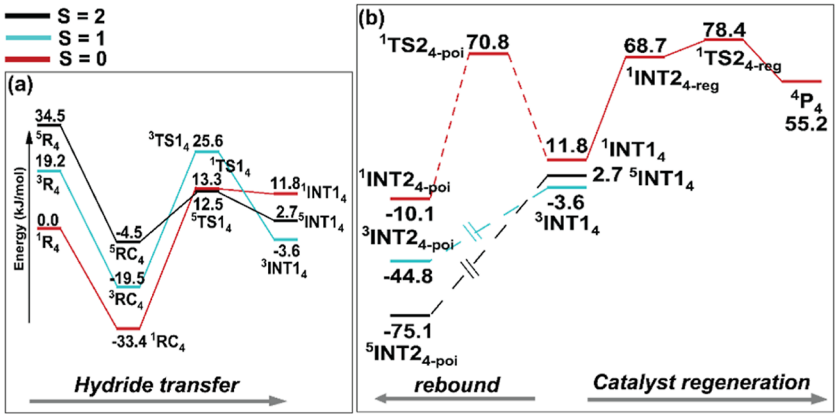

Figure 6. DFT computed energy profile diagram (kJ/mol) for (a) the hydride transfer followed by the (b) catalyst regeneration vs the formate rebound pathway in the catalytic hydrogenation of CO_2 by **4**.

role similar to the one described with the electric field rationalizing the observed experimental values.

Mechanism of Base-Assisted Hydrogenation of CO_2 by 4. A nucleophilic hydride trans to the methyl group of $PN^{Me}P$ pincer participates in the activation of CO_2 in **4** (Scheme S2). As mentioned earlier, all spin states in **4** are close lying and likely to compete in the reaction mechanism (Figure 6). Although the approach of CO_2 is exothermic in all spin states and the spin-state ordering [$^5RC_4$ (−4.5 kJ/mol) >$^3RC_4$ (−19.5 kJ/mol) >$^1RC_4$ (−33.4 kJ/mol)] (Figure S9b−d) is similar to a free catalyst, the energy requirement for the hydride transfer step is the lowest in the quintet energy surface [17.0 kJ/mol ($^5RC_4$ → $^5TS1_4$)]. The energetic cost for the hydride transfer follows the order $^1TS_4$ (46.7 kJ/mol) >$^3TS_4$ (45.1 kJ/mol) >$^5TS1_4$ (17.0 kJ/mol). This lower energy of the quintet transition state suggests the presence of a two-state or a multistate reactivity in **4**. In the next step, the newly forming hydride bound $HCOO^-$ intermediate (*INT1*; Figure S10b−d) is found to have a triplet ground state (−3.6 kJ/mol) followed by a quintet (2.7 kJ/mol) and singlet (11.8 kJ/mol) state. This suggests the involvement of two minimum-energy-crossing points (MECP), first from S = 0 to S = 2 during the formation of *TS1* and later from S = 2 to the S = 1 conversion during the formation of *INT1*. These MECPs are likely to add significant energy penalties.[59,60] At $^5TS1_4$, the hydride is found to attack the electrophilic carbon from a distance of 1.726 Å (1.628 and 1.558 Å in S = 1 and S = 0 spin state, respectively; Figure S11b−d). In $^5INT1$, the H−C bond is completely formed, having a bond length of 1.206 Å (1.214 and 1.269 Å in S = 1 and S = 0 spin states, respectively). The catalytic poisoning step, that is, conversion of *INT1* to $INT2_{poi}$ (Figure S13b−d) via $TS2_{poi}$ (Figure S12b), is analyzed. Although at the S = 0 surface, this transition state was found to have a barrier of 70.8 kJ/mol, at S = 1 and S = 2 surfaces, extensive relaxed potential energy scans were performed, revealing that this step is barrierless. At the same time, the formation of $INT2_{reg}$ from *INT1* is endothermic by 68.7 kJ/mol at a low-spin state. Further down the catalytic cycle, the energy penalty increased even further with the $TS2_{reg}$ barrier of 78.4 kJ/mol at the S = 0 surface. This barrier height for the regeneration of the catalyst is significantly higher compared to other catalysts, suggesting a very slow reaction reducing the TON significantly (<10 vs 2270 for **1**). Much more than the difference in the barrier height, the real reason for a drastic reduction in the TON for **4** arises from the extremely facile catalytic poisoning step at the S = 1 and S = 2 spin surfaces, which leads to the formation of $INT2_{poi}$ predominantly. This leaves the only option for the regeneration of the catalyst to cleave the Fe−O bond, which is an energy-demanding process. Given a favorable MECP, the reaction is thus likely to get quenched soon, suggesting that TSR/MSR hinders the catalytic reaction—an observation that is contrary to the established fact on biomimic catalysts/enzymes.

Employing OEEF to Boost the Catalytic Efficiency in 4. Any catalyst like **4**, which is devoid of a strong donor ligand in their ligand architecture, can be expected to show diminished efficiency toward formate production. Strategically, the reaction TON in this catalyst where more than one spin states are involved can be increased by (i) lifting the energies of these high/intermediate state as compared to the S = 0 ground state in the free catalyst or (ii) making the catalytic poison step unfavorable in the high/intermediate spin surface with the simultaneous reduction in the energy barrier for the catalyst regeneration process. For the second scenario, two-state reactivity during *INT1* → $INT2_{poi}$ via $TS2_{poi}$ must be hindered, which is a complicated phenomenon. Can the use of OEEF help in this scenario by regulating the energetics of different spin states?

First, we have applied an electric field ranging from $\pm 1.5 \times 10^{-3}$ to $\pm 4.5 \times 10^{-3}$ au oriented along the Fe−H2 axis (Figure 3j) in the free catalyst **4**. It is found that by increasing the field strength in the −*z*-direction, the energy gap between the ground S = 0 and excited S = 2 spin states increases steadily from 34.5 kJ/mol (field-free state) to 102.4 kJ/mol in $+4.5 \times 10^{-3}$ au field. The higher separation between the LS and HS states in the $+4.5 \times 10^{-3}$ au field eliminates the participation of the S = 2 HS state in the reaction mechanism (Table S6). Here, the intermediate S = 1 spin state responds weakly in the presence of an electric field, and the energy gap between the ground state and first-excited intermediate S = 1 state remains smaller, indicating that the S = 1 spin state participates in further reaction mechanism.

Reaction energetics reveal that an electric field oriented along both the +*z* (Fe−H2 direction) and −*z* (H2−Fe direction) axes stimulates the *RCs* in S = 1 spin states significantly as compared to the S = 0 spin state. The stability of *RCs* decreases (or increases) with the field in the +*z*- (or −*z*-) direction drastically in the S = 1 spin surface (energy margin of 29.8 kJ/mol with the highest OEEF value of -4.5×10^{-3} au; Figure 7a). Similarly, the energy barrier for the hydride transfer

https://doi.org/10.1021/acs.inorgchem.2c04119
Inorg. Chem. 2023, 62, 2342−2358

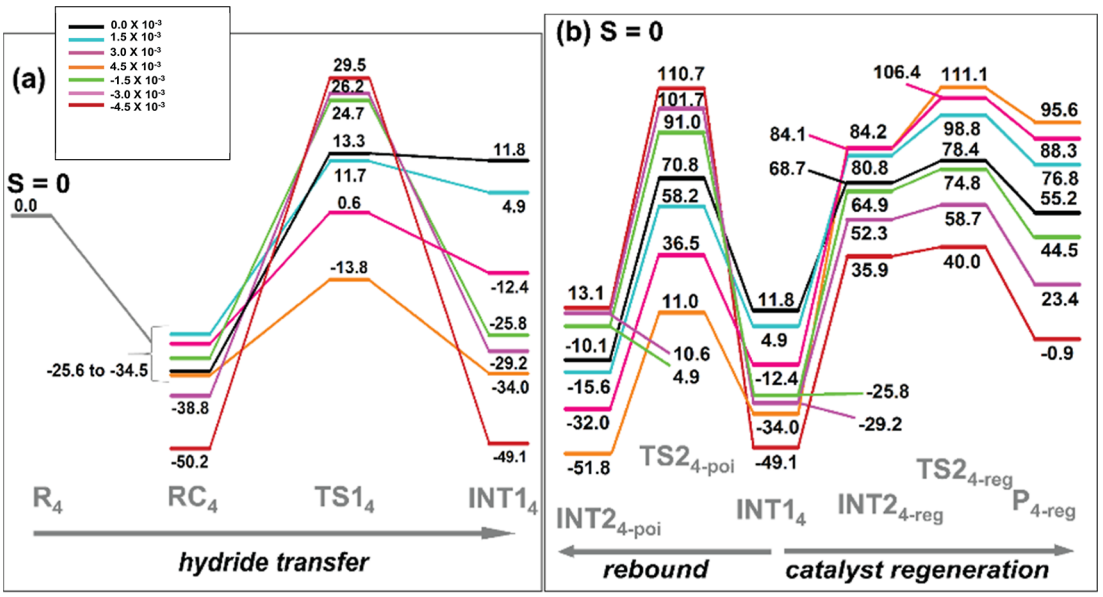

Figure 7. DFT computed energy profile diagram (kJ/mol) for (a) the hydride transfer followed by the (b) catalyst regeneration vs the formate rebound pathway in the catalytic hydrogenation of CO_2 by 4 in the S = 0 surface in different magnitudes of OEEF.

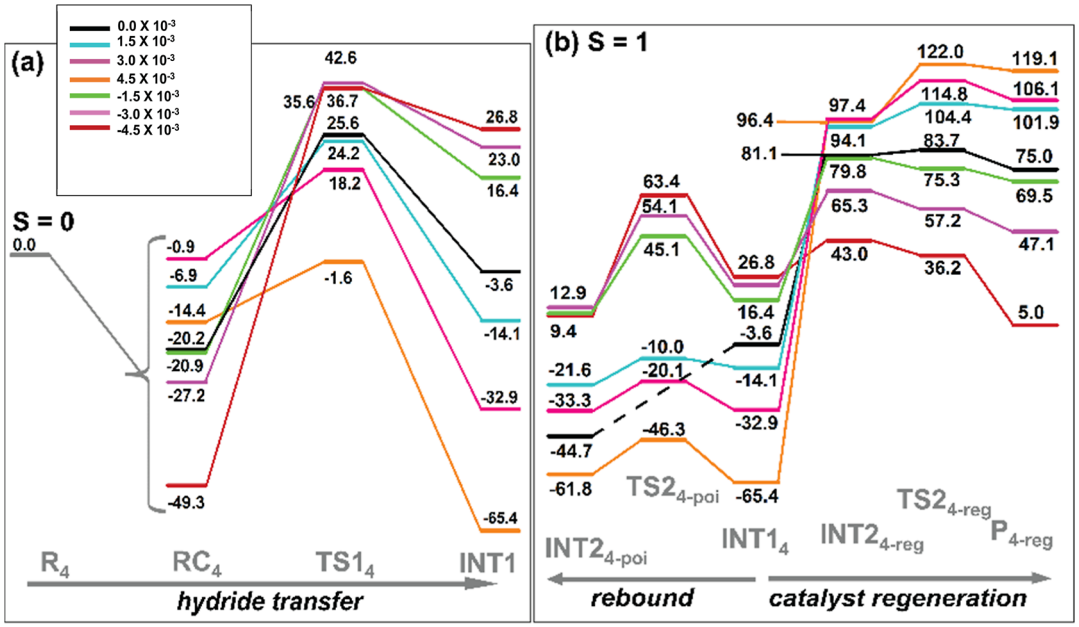

Figure 8. DFT computed energy profile diagram (kJ/mol) for (a) the hydride transfer followed by the (b) catalyst regeneration vs the formate rebound pathway in the catalytic hydrogenation of CO_2 by 4 in the S = 1 surface in different magnitudes of OEEF.

gradually decreases (reaches as low as 20.5/12.8 kJ/mol in the S = 0/1 spin state) along the +*z*-direction and increases steadily (reaches as high as 68.9/86.0 kJ/mol in the S = 0/1 spin state) along the −*z*-direction (Figures 7a and 8a). Although the barrier height calculated from the *RC*s in a specific field seems to be very high in the -4.5×10^{-3} au field, the barrier height from the free catalyst is <45 kJ/mol; therefore, the reaction can move forward in this field. Increasing the field strength in the +*z*-direction increases the negative charge on the hydride center (−0.048 to −0.063 in the S = 0 and −0.166 to −0.184 in the S = 1 spin state), so that hydride can attack from a longer (Fe)H···C(O2) distance (1.595 to 1.668 Å in S = 0 surface) (Tables S7 and S8). A similar trend is also followed in *INT1*, which gets stabilized with a gradual increase in the field strength along the +*z*-direction by a margin of 75.6 kJ/mol in S = 0 and S = 1 spin states, respectively.

In the next catalyst poison step, a barrier-less mechanism was observed in the S = 1 spin state in a field-free condition, which contributes to reduced efficiency. Although there was a significant rebound barrier in the S = 0 surface, it also competed with a similar barrier height (70.8 vs 68.7 kJ/mol) for the catalyst regeneration. Therefore, in a field-free condition, the higher-excited intermediate spin state plays a more significant role compared to the ground spin state in dictating efficiency. Interestingly, in both spin states, applying an electric field in the −*z*-direction gradually reduced the energy barrier for the catalyst regeneration process and

https://doi.org/10.1021/acs.inorgchem.2c04119
Inorg. Chem. 2023, 62, 2342−2358

simultaneously lifted the formate rebound barrier. Calculations reveal that at a field of -4.5×10^{-3} au, the catalyst regeneration barrier is decreased to 40.0 kJ/mol from 78.4 kJ/mol (field-free state) in the S = 0 spin state. At the same time, the energy requirement for the formate rebound increases to 110.7 kJ/mol, which was 70.8 kJ/mol in the field-free state. A similar scenario is observed in the intermediate S = 1 state. In the S = 1 surface, the energy barrier for the catalyst regeneration in -4.5×10^{-3} au is even lower than the barrier obtained for the S = 0 state (36.2 kJ/mol). In the same field, the energy penalty for the catalyst poison step increases from barrier-less (field-free) to 63.4 kJ/mol. A completely reverse scenario is observed with the electric field in the opposite direction.

The $TS2_{reg}$ geometries reveal that with the variation of OEEF in the $-z$-direction, the $H_p \cdots H_d$ distance decreases (0.946 to 0.915 and 0.947 to 0.905 Å in S = 0 and S = 1 states, respectively, for -1.5×10^{-3} Å au to -4.5×10^{-3} au field) with a gradual increase in the $H_d \cdots N(Pyrr)$ distance (1.482 to 1.533 and 1.385 to 1.447 Å in S = 0 and S = 1 states, respectively, for -1.5×10^{-3} Å au to -4.5×10^{-3} au field) (Table S7 and S8). The negative charge on the N(*Pyrr*) atom also increases to −0.685 (−0.683 in S = 1) at 4.5×10^{-3} au from −0.679 (−0.678) at -1.5×10^{-3} au (Tables S9 and S10). All these parameters indicate that the field along the negative z-direction enables attacks from a longer $H_d \cdots N(Pyrr)$ distance, facilitating the catalyst regeneration in both spin states. By increasing the field strength in the negative z-direction, the C−O(formate) bond distances decrease (1.238/1.257 to 1.237/1.253 Å from $+1.5 \times 10^{-3}$ Å au to -4.5×10^{-3} au field), increasing the C−O double bond character, therefore hampering the C−O rotational motion required to facilitate the formate rebound transition state. This led to an easier rebound in the more positive field and hindered the rebound in the more negative field. Moreover, the charge separation between the metal center and $O_{formate}$ decreases toward the -4.5×10^{-3} au field, hampering the catalytic poisoning. The catalyst regeneration versus catalyst poison energetics in various applied fields indicate that in both spin states, the application of a field in the $-z$-direction (H2−Fe direction) facilitates the catalyst regeneration process; therefore, it can be helpful in increasing the reaction TON.

The above studies show that OEEF not only regulate or control the selectivity or reactivity of a particular reaction but also capable to alter the energetics of various spin states. In the absence of OEEF, **4** was found to be unreactive due to the participation of high-lying spin states, which was contradictory to the conventional two-state reactivity in Fe(IV)═O species. However, with the application of an electric field, we are able to alter the reactivity of these high-lying states. First, we have successfully made the HS state inaccessible in the reaction mechanism by increasing crystal field stabilization energy with the help of OEEF, therefore mimicking the role of a strong field ligand. Second, we were able to alter the electronic flow in such a way that the high-lying intermediate state and low-spin states behave similarly, resulting in lower catalyst regeneration energy. Even at a certain electric field value (-4.5×10^{-3} au), the S = 1 spin state crosses the S = 0 state during $TS2_{reg}$, following a two-state reactivity mechanism which results in a decrease in the regeneration barrier, leading to higher efficiency. Therefore, for the first time, we have shown the response of various spin states in the presence of OEEF.

Role of Multiconfigurational Mixing in Controlling the Reaction Efficiency. Although the reaction mechanism studied occurs in the closed-shell S = 0 spin state, we performed multiconfigurational ab initio CASSCF calculations to assess and analyze the role of the other S = 0 state in the reactivity and to see if there are any configurational mixing which have been witnessed by us and others while studying the reactivity of Mn-oxo species.[61−63] Particularly, we performed *ab initio* calculations on $TS2_{1\text{-}reg}$ and $TS2_{1\text{-}poi}$, which are the pivotal steps in the reaction mechanism. Our calculations yield, as expected $(d_{xy})^2(d_{xz})^2(d_{yz})^2$ is the ground state with another open-shell singlet $(d_{xy})^2(d_{xz}, d_{yz})^3(d_{z^2})^1$, is found to mix strongly with the ground state wavefunction (Figure 3k). This is a surprising twist, as open-shell singlet states are not expected to influence the reactivity and therefore have generally been neglected. The ground state wave function of $TS2_{1\text{-}reg\text{-}DBU}$ is composed of 71.3% contribution from the closed-shell S = 0 configurations, with 25.8% contribution from another open-shell S = 0 state, suggesting a significant mixing of the ground state with the higher excited state of the same spin multiplicity. From the catalyst regeneration transition state, it is evident that the amine base is directly involved in the H−H bond cleavage, with the H···N(base) bond distance falling within <1.5 Å. As H_2 is directly attached to the Fe atom, this alters the electronic configuration as the H···H bond elongates. The open-shell contribution in $TS2_{1\text{-}reg\text{-}pyrr}$ and $TS2_{1\text{-}reg\text{-}mor}$ is estimated to be 37.3 and 49.8%, which are in line with the energy barrier for these transition states. On the contrary, the ground state configuration of $TS2_{1\text{-}poi\text{-}DBU}$ consists of a negligible (<1%) amount of open-shell contribution. The ground state configuration of $TS2_{1\text{-}poi\text{-}mor}$ consists of only 8.4% closed-shell confirmation with the lion's share (73.7%) from the open-shell one, suggesting that catalytic poisoning is predominantly routed via the open-shell singlet state (Table S11). In the catalytic poison transition state (given in Figure S7), the bond distance between the base and the formate group is 2.085, 2.163, and 5.385 Å, respectively, for $TS2_{1\text{-}poi\text{-}pyrr}$, $TS2_{1\text{-}poi\text{-}mor}$, and $TS2_{1\text{-}poi\text{-}DBU}$. This suggests that the base with less basicity and smaller size can approach closer to the formate to facilitate the rebound mechanism, while for the DBU, which is larger in size, this is challenging. Therefore, $TS2_{1\text{-}poi\text{-}DBU}$ is associated with the highest barrier for catalyst poisoning than pyrrolidine and morpholine. Also, a larger distance between DBU and formate results in a negligible amount of open-shell contribution, affecting the closed-shell configuration the least. If we compare and contrast the barrier height and the degree of mixing, it is clear that the greater the percentage of open-shell singlet, the larger will be the energy penalty for the catalyst regeneration transition state. This is correlated to the crystal field splitting, nature of transition state, and external stimuli such as Bronsted acids and bases. Among the three reactions studied, clearly open-shell singlet character for DBU is least at the catalytic regeneration step and the most at the catalytic poisoning step, making catalyst regeneration facile, aiding larger TON numbers. For morpholine, on the other hand, the open-shell singlet character is relatively higher both at the catalytic regeneration step and at the catalytic poisoning step, making it the least efficient reaction.

A closer look at why the BH_3 results in a lower barrier reveals a less steric strain at the transition state $TS2_{1\text{-}reg\text{-}BH3}$ (lower deformation energy 112.8 vs 129.9 kJ/mol in the absence of BH_3). Further, at this particular transition state, a

https://doi.org/10.1021/acs.inorgchem.2c04119
Inorg. Chem. 2023, 62, 2342−2358

less percentage of open-shell singlet (14.5 vs 37.3% in the presence/absence of BH_3) is found, leading to a lower barrier. In the presence of LiOTf, the open-shell singlet configuration to the closed-shell configuration is found to be the lowest (2% contribution from the open-shell configuration to 94% from the closed-shell configuration) in $TS2_{reg\text{-}LiOTf}$, indicating the lowest energy barrier for catalyst regeneration. Thus, the presence of Lewis acid BH_3 and LiOTf in the solution enhances the catalytic ability by offering less steric strain at the rate-determining step and also reduces the flexibility of the electronic structure, favoring the overall reaction rate/TONs. Although the BH_3 reduces the barrier, a stronger base such as DBU reduces the barrier even further (48.9 vs 38.2 kJ/mol in pyrrolidine-BH_3 and DBU, respectively), rationalizing the larger efficiency observed with DBU compared to pyrrolidine in the presence of Lewis acid (6900 vs 4620).[56,57] The lower barriers for DBU stem from very less steric strain at the transition state, though the electronic factor (percentage of open-shell singlet character) is not that favorable. Similar to the external additives, the effect of the external electric field is observed in terms of closed-shell versus open-shell configurations in the different electric fields. The CASSCF calculated mixing of various singlet states suggests that in $TS2_{reg}$ along the $-z$-direction, the electronic flexibility diminishes drastically compared to the filed free state. After the -1.5×10^{-3} au field, the mixing is the least (<3% contribution from the open-shell configuration) among all computations performed, suggesting that this multiconfigurational mixing can be used as a qualitative tool to assess the reactivity order as seen in C−H bond activation by metal-oxo species.

Correlation to Experiments. (i) Experimental studies suggest that all four catalysts (**1**−**4**) react via the same reaction mechanism for the reductive CO_2 hydrogenation reaction, and our study solidifies this observation, with **2** acting as a co-catalyst of **1**. (ii) Our theoretically predicted barrier heights (rebound vs regeneration) agree with experimental observations that **2** shows the highest TON of 2440, followed by **1** (2270). The efficiency of **4** is the lowest, with the TON less than 10. (iii) Experiments suggest the formation of [(^{iPr}PNP)-Fe(H)CO(HCO_2)] species as the resting state for the formate production, and removal of the product from this species is found to be extremely difficult without strong external stimuli such as Li^+ ion. Even in the presence of a strong base and long reaction hours, the reaction was found not to proceed further. All these experimental observations strongly supported our proposal of catalytic poisoning. (iv) Experiments suggest that the catalyst regeneration step is rate determining, and our mechanism and computed energetics support this argument, providing confidence in the computed energetics.

The experimental TON and turnover frequency for the reaction of 1 are reported to be 3.897×10^4 and 1.841×10^4 h^{-1}, respectively, in 7.5:1 DBU and LiOTf conditions.[56] The reported TON value is 2790 in excess DBU. Therefore, $t_{1/2}$ of those reactions will be 1.467 as per the established literature.[64] As the fate of the reaction, whether it will regenerate the catalyst or undergo rebound, is decided by INT1 (Fe−H(formate) species), the catalyst regeneration transition state ($TS2_{reg}$) is considered as the rate-determining transition state (TDTS) and INT1 species as the rate-determining intermediate (TDI) during the CO_2 hydrogenation to formate. The energy barrier [TDTS−TDI] for **1** in DBU is found to be 58.0 kJ/mol. Using energetic span approximation,[64,65] we have calculated the TOF for the above reaction, which is 424.1 h^{-1}. Further, we have calculated TON from the value of TOF, which is estimated to be 900. It is noted that these quantitative values are based on the energy barriers calculated in the presence of 1:1 Lewis base DBU and Fe. Therefore, an underestimation of the calculated TON is reasonable as it is calculated only in the presence of DBU, while the reported values are in the presence of LiOTf (38,970) and excess DBU (2790 h^{-1}). Therefore, we have estimated the TOF in the presence of LiOTf based on the energy barrier of 43.0 kJ/mol. In the presence of Lewis acid, the first hydride transfer step is considered rate limiting. The calculated TOF and TON in 1:1 DBU and LiOTf (i.e., with 50% LiOTF) are 2.54×10^5 and 5.37×10^5 h^{-1}, respectively. These values are an order of magnitude larger than the experimental TOF (1.841×10^4 h^{-1}). However, as experimental conditions are 1:7 (LiOTf/DBU), with excess DBU and lower LiOTf, the TOF is expected to be reduced, and this is consistent with our calculated values.

DISCUSSION

In this work, using a combination of the DFT and *ab initio* CASSCF calculations coupled with studies utilizing an OEEF, we have explored the mechanism of CO_2 hydrogenation to formate by earth-abundant Fe catalysts exhibiting TONs as high as 60,000.[56,57] DFT calculations yield an S = 0 spin state as the ground state for all four catalysts **1**−**4**, with other S = 1 and S = 2 states lying significantly higher in energy for **1**−**3** and a relatively in accessible range for **4**, suggesting a possible TSR activity.

Chemical Ways to Boost the Reaction Efficiency. This mechanistic study brings forth various design clues for efficient CO_2 hydrogenation: (i) the reductive CO_2 hydrogenation initiated by the approach of the CO_2 molecule to the periphery of the catalyst along with the base, resulting in the formation of a stable *RC* species, {LFe(H)(X)[CO_2]} (X = H, BH_4). At this *RC*, there are several noncovalent interactions observed by the peripheral isopropyl groups [(^{i}*pr*$_2$)C−H···O(CO)] and the pyrrolidine (morpholine or DBU) base as [(*Pyrr*)N−H···O(CO)], which is found to activate CO_2 weakly even before the hydride transfer step kicks in. This illustrates the importance of alkyl substituents and the utilization of a strong base in CO_2 hydrogenation. While this finding applies to all catalysts **1**−**4**, several base metal catalysts that activate CO_2 reported in the literature were found to possess such substituents in the ligand periphery,[25,66−73] suggesting the generic applicability of this step in CO_2 activation. Our findings are contrary to the general understanding that steric crowding using the alkyl tethering groups is expected to hinder catalytic efficiency. For CO_2 activation, on the other hand, these tethering groups are an essential ingredient in enhancing efficiency, thereby establishing a hitherto unknown strategy in the ligand design in CO_2 activation.[6,26,69,71,72] (ii) In the presence of external stimuli like Li^+ salts, the catalyst poison step is found to be very facile, forming the LFe···O−HCO ($INT2_{poi}$) species. In the next step, the Fe−O bond in $INT2_{poi}$ gets cleaved with the help of Lewis acid, which eventually reacts with the molecular hydrogen and undergoes a catalyst regeneration process. The reaction TON is found to be dependent on the following factors: (a) energetic gain during the *RC* formation and (b) energy loss in the catalyst generation process. Higher factor (a) and lower factor (b) dictate the reaction efficiency in the presence of external stimuli. Thus, with the apt Lewis acid such as LiOTf, the catalyst is

https://doi.org/10.1021/acs.inorgchem.2c04119
Inorg. Chem. 2023, 62, 2342−2358

regenerated from the catalytic poisoning, thus avoiding the catalytic poisoning step altogether. As this is the important fundamental step that diminishes the efficiency, its absence boosts the reaction efficiency significantly. This, coupled with additional stability of *RC* that eases further energy requirements, makes LiOTf a potent additive to boost TON to as high as 60,000. (iii) While catalysts **1**−**3** react via a single energy surface (S = 0), catalyst **4** reacts via TSR/MSR. The involvement of various spin states in the reactivity is attributed to the absence of strong-field carbonyl ligation to Fe in **4**. The S = 2 HS and S = 1 IS states lie closer to the ground S = 0 low-spin state in **4**. These slightly high-lying HS/IS spin states are found to participate in the reaction further and even control the reaction course. The barrier-less formate rebound step in the high-lying HS/IS state monopolizes the reaction toward the catalyst poisoning step, hindering the product formation and lowering the TON. This suggests that any ligand that offers a weaker ligand field results in catalytic poisoning. This has greater implications beyond these catalysts studied. Earlier CO_2 hydrogenation by the Co-catalyst reported by Liu and co-workers reveals weak/no reactivity for the Co catalyst having a PNN ligand framework compared to the PPN ligand framework. The Co-PNN ligand framework is known to yield a very small gap among the spin states or even stabilize HS as the ground state,[74] suggesting strong involvement of TSR. In these complexes, the TSR hindrance is expected to be greater than that found in **4** (note that **4** has a PNP framework), leading to no reactivity. (iv) Further, it is found that a stronger Bronsted base not only lowers the barrier for the heterogeneous H_2-cleavage but also spikes the formate rebound, facilitating the formate release and the catalyst regeneration step by lowering the flexibility in an electronic configuration. This is also found to be true in many of the CO_2 hydrogenation reactions, including that of Beller and co-workers.[72] (v) In the present study, we have shown the dependency of the intrinsic barrier of various transition states during CO_2 hydrogenation to formate production on two factors: steric requirement and electronic flexibility of the ground state wavefunction. The first factor is straightforward; the reaction barrier depends linearly on the extent of deformation in the transition state structures compared to the reactants. The second factor is the presence of multi-configurational states in the ground state wave function. It is observed that although the ground state of the electron-rich Fe(II) species is composed of a closed-shell configuration, the probability of the admixing of the higher excited open-shell singlet states cannot be ignored. Our ab initio CASSCF calculation has depicted this scenario and concluded that the higher the mixing of the open-shell singlet state to the closed-shell single state, the higher will be the energy barrier. Therefore, higher electronic flexibility hinders reactivity.

Non-Chemical Way to Boost the Reaction Efficiency by Employing OEEFs. The response of various stationary points during the CO_2 hydrogenation reaction catalyzed by **1** has been noted towards the OEEF as an external stimulus. Our motive was to mimic the role of Lewis acids during the catalytic hydrogenation reaction by facilitating the heterogeneous H_2-splitting step and at the same time retarding the catalyst poison step with the help of OEEFs. Our study affirms that the application of an electric field of 4.5×10^{-3} au along the H1−Fe−H2 direction (−*z*-axis) is suitable for enhancing the catalytic efficiency as the energy requirement for the catalyst regeneration is the least in this particular direction. At the same time, the same amount of electric field increases the energy penalty for the formate rebound drastically. The alternation in the reaction rate in the presence of OEEFs is attributed to the occurrence of the following factors: (i) an electric field along both +*z*- and −*z*-directions strengthens the noncovalent (*Pyrr*)N−H···O(CO), ($^{i}pr_2$)C−H···O(CO), and (Fe)H1···C(O2) interactions, anchoring the CO_2 molecule to the catalyst strongly in comparison to the field-free state. The stronger hold on the CO_2 molecule contributed to either the catalyst regeneration or catalyst rebound process depending on the direction of an electric field applied. (ii) In the +*z*-direction, the hydride transfer to the CO_2 barrier increases due to the accumulation of negative charges on the hydride, and the reverse is true for the electric field in the −*z*-direction. In the −*z*-direction, the hydride transfer barrier increases as much as 77.1 kJ/mol, below which which all other transition states fall, making this step rate limiting while applying an electric field along the H1−Fe−H2 direction. (iii) In the −*z*-direction, with increasing OEEF strength, the H···H distances become shortened with the increase in the charge on N(*Pyrr*), which makes the N(*Pyrr*) moiety abstract the distal hydride (H_d) from a longer distance, resulting in the reduction of steric crowing as well as barrier height. (iv) In the −*z*-direction, with increasing OEEF strength, the negative charge on the metal increases, along with the decrease in the negative dipole on the rebound oxygen, making the Fe−O bond formation in the subsequent intermediate difficult. If we calculate the EP ratio in the presence of the apt OEEF, it is found to be 4.14, which is even higher than the value obtained in the presence of LiOTf, suggesting a non-chemical way to tune the TON even beyond 60,000. This finding is very new in the case of the catalytic reactivity of electron-rich transition metal catalysts (Fe, Co, Ni, Pt, Ru, and Pd), which are believed to react via a single low-spin energy surface and raise a fundamental question about the true involvement of only closed-shell configurations,

The catalysts without any strong field ligands in their ligand architecture are found to be a bad candidate in terms of TON due to the participation of other excited states in the reaction mechanism. These higher excited states are found to favor the catalyst poisoning step over the catalyst regeneration process, therefore being toxic in terms of catalytic efficiency. Employing an OEEF in an apt direction can avoid all the issues mentioned, can boost the catalytic efficiency as high as the best catalyst, and avoid elaborate chemical modifications that are often required to improve the catalytic efficiency.

CONCLUSIONS

Herein, employing a combination of DFT and *ab initio* CASSCF method, we have studied the mechanism of reductive CO_2 hydrogenation to formate by PNP pincer-based earth-abundant Fe(II) catalysts, [(^{iPr}PN^{Me}P)FeH$_2$(CO)], [(^{iPr}PN^{Me}P)FeH(CO)(BH$_4$)], [(^{iPr}PN^{H}P)FeH(CO)(BH$_4$)], and [(^{iPr}PN^{Me}P)FeH(BH$_4$)], which exhibit a TON varying from 10 to as high as 60,000—one of the highest reported for this type of reaction. Despite having a similar ligand architecture, the variation observed in TON is puzzling, and this is universally true also for other catalysts based on Fe and Co. Our calculations unveil three fundamental mechanistic steps: (i) anchoring CO_2 in the vicinity of the metal, (ii) regeneration of the catalyst upon formate formation, and (iii) catalytic poisoning via formate rebound. Attempts to facilitate steps (i) and (ii) and disfavor step (iii) were found to yield

https://doi.org/10.1021/acs.inorgchem.2c04119
Inorg. Chem. 2023, 62, 2342−2358

greater efficiency. The TON observed for the catalysts studied here were rationalized based on their ligand architecture and the associated energy penalties. Further, the role of additives such as Lewis acid and strong bases in influencing the efficiency was correlated to a lower barrier for regeneration and a higher barrier for poisoning, suggesting a generic mechanism that can also be adapted to other metals. Our study also offers several important design clues to improve the TONs for this reaction: (a) facilitating C−H···O(CO) and N−H···O(CO) interactions in the ligand framework, (b) avoiding the metal−ligand cooperativity containing metal−NH secondary amines to reduce the chance of catalytic poisoning, and (c) avoiding a paramagnetic ground/close-lying excited states as it facilitates faster catalytic poisoning. Thus, the two-state reactivity—a celebrated concept to enhance the efficiency of metal-oxo species—is found to be lethal for this reaction. A strong ligand field around the metal center with the π-acceptor ligand is desired as it destabilizes the HS states, leading to enhanced efficiency. (d) Even if a singlet ground state results, the catalyst that exhibits strong mixing with other open-shell singlet configurations in the catalyst regeneration process is found to diminish the reactivity. Thus, the presence of Lewis acids such as BH_3/LiOTf was found to offer less mixing of various singlet states to the ground state, facilitating greater reactivity. (e) A non-chemical way to fine-tune the catalyst based on an OEEF is proposed. In the present catalyst studied, a small electric field in the opposite direction to the reaction axis (in the present case, along H1−Fe−H2) was found to enhance the catalytic efficiency significantly even beyond the reported TONs. This process eliminates the need to tune the ligand architecture and optimize the reaction conditions via various bases/acids to boost the TONs and henceforth has scope beyond the examples presented. The proposed mechanism, as well as the computed TONs and TOFs for some of the catalysts, is consistent with the experimental trend.

■ ASSOCIATED CONTENT

Supporting Information

The Supporting Information is available free of charge at https://pubs.acs.org/doi/10.1021/acs.inorgchem.2c04119.

Optimized geometries, structural parameters and computed charges, and inputs employed for the calculations along with the final optimized coordinates for all the species reported (PDF)

All the coordinates are also given as ASCII file (TXT)

■ AUTHOR INFORMATION

Corresponding Author

Gopalan Rajaraman − *Department of Chemistry, Indian Institute of Technology Bombay, Mumbai 400076, India;* orcid.org/0000-0001-6133-3026; Email: rajaraman@chem.iitb.ac.in

Author

Asmita Sen − *Department of Chemistry, Indian Institute of Technology Bombay, Mumbai 400076, India*

Complete contact information is available at: https://pubs.acs.org/10.1021/acs.inorgchem.2c04119

Notes

The authors declare no competing financial interest.

■ ACKNOWLEDGMENTS

We thank DST and SERB (CRG/2022/001697; SB/SJF/2019-20/12) for funding. A.S. thanks CSIR for a fellowship.

■ REFERENCES

(1) Dincer, I. Environmental impacts of energy. *Energy Policy* **1999**, *27*, 845−854.

(2) Lewis, N. S.; Nocera, D. G. Powering the planet: Chemical challenges in solar energy utilization. *Proc. Natl. Acad. Sci. U.S.A.* **2006**, *103*, 15729−15735.

(3) Dimitratos, N.; Lopez-Sanchez, J. A.; Hutchings, G. J. Green catalysis with alternative feedstocks. *Top. Catal.* **2009**, *52*, 258−268.

(4) Cokoja, M.; Bruckmeier, C.; Rieger, B.; Herrmann, W. A.; Kühn, F. E. Transformation of Carbon Dioxide with Homogeneous Transition-Metal Catalysts: A Molecular Solution to a Global Challenge? *Angew. Chem., Int. Ed.* **2011**, *50*, 8510−8537.

(5) Appel, A. M.; Bercaw, J. E.; Bocarsly, A. B.; Dobbek, H.; DuBois, D. L.; Dupuis, M.; Ferry, J. G.; Fujita, E.; Hille, R.; Kenis, P. J.; Kerfeld, C. A.; Morris, R. H.; Peden, C. H. F.; Portis, A. R.; Ragsdale, S. W.; Rauchfuss, T. B.; Reek, J. N. H.; Seefeldt, L. C.; Thauer, R. K.; Waldrop, G. L. Frontiers, opportunities, and challenges in biochemical and chemical catalysis of CO2 fixation. *Chem. Rev.* **2013**, *113*, 6621−6658.

(6) Federsel, C.; Jackstell, R.; Beller, M. State-of-the-Art Catalysts for Hydrogenation of Carbon Dioxide. *Angew. Chem., Int. Ed.* **2010**, *49*, 6254−6257.

(7) Bozell, J. J.; Patel, M. K.*Feedstocks for the Future*; ACS: New York, 2006.

(8) Weilhard, A.; Argent, S. P.; Sans, V. Efficient carbon dioxide hydrogenation to formic acid with buffering ionic liquids. *Nat. Commun.* **2021**, *12*, 231.

(9) Gerack, C. J.; McElwee-White, L. Formylation of amines. *Molecules* **2014**, *19*, 7689−7713.

(10) Burkart, M. D.; Hazari, N.; Tway, C. L.; Zeitler, E. L. Opportunities and challenges for catalysis in carbon dioxide utilization. *ACS Catal.* **2019**, *9*, 7937−7956.

(11) Heimann, J. E.; Bernskoetter, W. H.; Hazari, N.; Mayer, J. M. Acceleration of CO2 insertion into metal hydrides: ligand, Lewis acid, and solvent effects on reaction kinetics. *Chem. Sci.* **2018**, *9*, 6629−6638.

(12) Heimann, J. E.; Bernskoetter, W. H.; Hazari, N. Understanding the individual and combined effects of solvent and lewis acid on CO2 insertion into a metal hydride. *J. Am. Chem. Soc.* **2019**, *141*, 10520−10529.

(13) Bernskoetter, W. H.; Hazari, N. Reversible hydrogenation of carbon dioxide to formic acid and methanol: Lewis acid enhancement of base metal catalysts. *Acc. Chem. Res.* **2017**, *50*, 1049−1058.

(14) Liu, Q.; Wu, L.; Jackstell, R.; Beller, M. Using carbon dioxide as a building block in organic synthesis. *Nat. Commun.* **2015**, *6*, 5933.

(15) Huff, C. A.; Sanford, M. S. Catalytic CO2 hydrogenation to formate by a ruthenium pincer complex. *ACS Catal.* **2013**, *3*, 2412−2416.

(16) Cornils, B.; Herrmann, W. A.*Aqueous-Phase Organometallic Catalysis: Concepts and Applications*; John Wiley & Sons, 2004.

(17) Hull, J. F.; Himeda, Y.; Wang, W.-H.; Hashiguchi, B.; Periana, R.; Szalda, D. J.; Muckerman, J. T.; Fujita, E. Reversible hydrogen storage using CO2 and a proton-switchable iridium catalyst in aqueous media under mild temperatures and pressures. *Nat. Chem.* **2012**, *4*, 383−388.

(18) Maenaka, Y.; Suenobu, T.; Fukuzumi, S. Catalytic interconversion between hydrogen and formic acid at ambient temperature and pressure. *Energy Environ. Sci.* **2012**, *5*, 7360−7367.

(19) Himeda, Y.; Onozawa-Komatsuzaki, N.; Sugihara, H.; Arakawa, H.; Kasuga, K. Half-Sandwich Complexes with 4,7-Dihydroxy-1,10-phenanthroline: Water-Soluble, Highly Efficient Catalysts for Hydrogenation of Bicarbonate Attributable to the Generation of an Oxyanion on the Catalyst Ligand. *Organometallics* **2004**, *23*, 1480−1483.

(20) Laurenczy, G.; Joó, F.; Nádasdi, L. Formation and Characterization of Water-Soluble Hydrido-Ruthenium(II) Complexes of 1,3,5-Triaza-7-phosphaadamantane and Their Catalytic Activity in Hydrogenation of CO2 and HCO3- in Aqueous Solution. *Inorg. Chem.* **2000**, *39*, 5083−5088.
(21) Drake, J. L.; Manna, C. M.; Byers, J. A. Enhanced carbon dioxide hydrogenation facilitated by catalytic quantities of bicarbonate and other inorganic salts. *Organometallics* **2013**, *32*, 6891−6894.
(22) Zhang, L.; Han, Z.; Zhao, X.; Wang, Z.; Ding, K. Highly Efficient Ruthenium-Catalyzed N-Formylation of Amines with H2and CO2. *Angew. Chem.* **2015**, *127*, 6284−6287.
(23) Comba, P.; Gahan, L. R.; Hanson, G. R.; Maeder, M.; Westphal, M. Carbonic anhydrase activity of dinuclear CuIIcomplexes with patellamide model ligands. *Dalton Trans.* **2014**, *43*, 3144−3152.
(24) Sabater, S.; Menche, M.; Ghosh, T.; Krieg, S.; Rück, K. S.; Paciello, R.; Schäfer, A.; Comba, P.; Hashmi, A. S. K.; Schaub, T. Mechanistic investigation of the nickel-catalyzed carbonylation of alcohols. *Organometallics* **2020**, *39*, 870−880.
(25) Federsel, C.; Ziebart, C.; Jackstell, R.; Baumann, W.; Beller, M. Catalytic Hydrogenation of Carbon Dioxide and Bicarbonates with a Well-Defined Cobalt Dihydrogen Complex. *Chem.—Eur. J.* **2012**, *18*, 72−75.
(26) Daw, P.; Chakraborty, S.; Leitus, G.; Diskin-Posner, Y.; Ben-David, Y.; Milstein, D. Selective N-formylation of amines with H2 and CO2 catalyzed by cobalt pincer complexes. *ACS Catal.* **2017**, *7*, 2500−2504.
(27) Mondal, B.; Neese, F.; Ye, S. Control in the rate-determining step provides a promising strategy to develop new catalysts for CO2 Hydrogenation: a local pair natural orbital coupled cluster theory study. *Inorg. Chem.* **2015**, *54*, 7192−7198.
(28) Mondal, B.; Neese, F.; Ye, S. Toward rational design of 3d transition metal catalysts for CO2 hydrogenation based on insights into hydricity-controlled rate-determining steps. *Inorg. Chem.* **2016**, *55*, 5438−5444.
(29) Chakraborty, S.; Lagaditis, P. O.; Förster, M.; Bielinski, E. A.; Hazari, N.; Holthausen, M. C.; Jones, W. D.; Schneider, S. Well-defined iron catalysts for the acceptorless reversible dehydrogenation-hydrogenation of alcohols and ketones. *ACS Catal.* **2014**, *4*, 3994−4003.
(30) Bielinski, E. A.; Förster, M.; Zhang, Y.; Bernskoetter, W. H.; Hazari, N.; Holthausen, M. C. Base-free methanol dehydrogenation using a pincer-supported iron compound and Lewis acid co-catalyst. *ACS Catal.* **2015**, *5*, 2404−2415.
(31) Ahlquist, M. S. G. Iridium catalyzed hydrogenation of CO2 under basic conditions—Mechanistic insight from theory. *J. Mol. Catal. A: Chem.* **2010**, *324*, 3−8.
(32) Yang, X. Hydrogenation of carbon dioxide catalyzed by PNP pincer iridium, iron, and cobalt complexes: a computational design of base metal catalysts. *ACS Catal.* **2011**, *1*, 849−854.
(33) Ogo, S.; Kabe, R.; Hayashi, H.; Harada, R.; Fukuzumi, S. Mechanistic investigation of CO2 hydrogenation by Ru(ii) and Ir(iii) aqua complexes under acidic conditions: two catalytic systems differing in the nature of the rate determining step. *Dalton Trans.* **2006**, *39*, 4657−4663.
(34) Jeletic, M. S.; Helm, M. L.; Hulley, E. B.; Mock, M. T.; Appel, A. M.; Linehan, J. C. A cobalt hydride catalyst for the hydrogenation of CO2: pathways for catalysis and deactivation. *ACS Catal.* **2014**, *4*, 3755−3762.
(35) Shaik, S.; Mandal, D.; Ramanan, R. Oriented electric fields as future smart reagents in chemistry. *Nat. Chem.* **2016**, *8*, 1091−1098.
(36) Shaik, S.; Danovich, D.; Joy, J.; Wang, Z.; Stuyver, T. Electric-field mediated chemistry: uncovering and exploiting the potential of (oriented) electric fields to exert chemical catalysis and reaction control. *J. Am. Chem. Soc.* **2020**, *142*, 12551−12562.
(37) Shaik, S.; de Visser, S. P.; Kumar, D. External electric field will control the selectivity of enzymatic-like bond activations. *J. Am. Chem. Soc.* **2004**, *126*, 11746−11749.
(38) Joy, J.; Stuyver, T.; Shaik, S. Oriented external electric fields and ionic additives elicit catalysis and mechanistic crossover in oxidative addition reactions. *J. Am. Chem. Soc.* **2020**, *142*, 3836−3850.
(39) Wang, C.; Danovich, D.; Chen, H.; Shaik, S. Oriented external electric fields: tweezers and catalysts for reactivity in halogen-bond complexes. *J. Am. Chem. Soc.* **2019**, *141*, 7122−7136.
(40) Tarrago, M.; Ye, S.; Neese, F. Electronic structure analysis of electrochemical CO2 reduction by iron-porphyrins reveals basic requirements to design catalysts bearing non-innocent ligands. *Chem. Sci.* **2022**, *13*, 10029−10047.
(41) Frisch, M.; Trucks, G.; Schlegel, H.; Scuseria, G.; Robb, M.; Cheeseman, J.; Scalmani, G.; Barone, V.; Petersson, G.; Nakatsuji, H.*Gaussian 16 C. 01*, 2016.
(42) Zhao, Y.; Truhlar, D. G. A new local density functional for main-group thermochemistry, transition metal bonding, thermochemical kinetics, and noncovalent interactions. *J. Chem. Phys.* **2006**, *125*, 194101.
(43) Hay, P. J.; Wadt, W. R. Ab initio effective core potentials for molecular calculations. Potentials for the transition metal atoms Sc to Hg. *J. Chem. Phys.* **1985**, *82*, 270−283.
(44) Verma, P.; Varga, Z.; Klein, J. E.; Cramer, C. J.; Que, L.; Truhlar, D. G. Assessment of electronic structure methods for the determination of the ground spin states of Fe(ii), Fe(iii) and Fe(iv) complexes. *Phys. Chem. Chem. Phys.* **2017**, *19*, 13049−13069.
(45) Tirado-Rives, J.; Jorgensen, W. L. Performance of B3LYP density functional methods for a large set of organic molecules. *J. Chem. Theory Comput.* **2008**, *4*, 297−306.
(46) Salomon, O.; Reiher, M.; Hess, B. A. Assertion and validation of the performance of the B3LYP★ functional for the first transition metal row and the G2 test set. *J. Chem. Phys.* **2002**, *117*, 4729−4737.
(47) Grimme, S. Density functional theory with London dispersion corrections. *Wiley Interdiscip. Rev.: Comput. Mol. Sci.* **2011**, *1*, 211−228.
(48) Zheng, J.; Xu, X.; Truhlar, D. G. Minimally augmented Karlsruhe basis sets. *Theor. Chem. Acc.* **2011**, *128*, 295−305.
(49) Marenich, A. V.; Cramer, C. J.; Truhlar, D. G. Universal solvation model based on solute electron density and on a continuum model of the solvent defined by the bulk dielectric constant and atomic surface tensions. *J. Phys. Chem. B* **2009**, *113*, 6378−6396.
(50) Bickelhaupt, F. M.; Houk, K. N. Analyzing Reaction Rates with the Distortion/Interaction-Activation Strain Model. *Angew. Chem., Int. Ed.* **2017**, *56*, 10070−10086.
(51) Ansari, M.; Senthilnathan, D.; Rajaraman, G. Deciphering the origin of million-fold reactivity observed for the open core diiron [HO-FeIII-O-FeIV·O]2+species towards C-H bond activation: role of spin-states, spin-coupling, and spin-cooperation. *Chem. Sci.* **2020**, *11*, 10669−10687.
(52) Singh, S.; Sunoj, R. B. Mechanism and Origin of Enantioselectivity in Nickel-Catalyzed Alkyl-Alkyl Suzuki Coupling Reaction. *J. Phys. Chem. A* **2019**, *123*, 6701−6710.
(53) Neese, F.; Wennmohs, F.; Becker, U.; Riplinger, C. The ORCA quantum chemistry program package. *J. Chem. Phys.* **2020**, *152*, 224108.
(54) Reiher, M. Douglas−Kroll−Hess Theory: a relativistic electrons-only theory for chemistry. *Theor. Chem. Acc.* **2006**, *116*, 241−252.
(55) Roos, B. O.The complete active space self-consistent field method and its applications in electronic structure calculations. *Advances in Chemical Physics: Ab Initio Methods in Quantum Chemistry Part 2*; Wiley Online Library, 1987; Vol. *69*, pp 399−445.
(56) Zhang, Y.; MacIntosh, A. D.; Wong, J. L.; Bielinski, E. A.; Williard, P. G.; Mercado, B. Q.; Hazari, N.; Bernskoetter, W. H. Iron catalyzed CO2hydrogenation to formate enhanced by Lewis acid co-catalysts. *Chem. Sci.* **2015**, *6*, 4291−4299.
(57) Jayarathne, U.; Hazari, N.; Bernskoetter, W. H. Selective iron-catalyzed N-formylation of amines using dihydrogen and carbon dioxide. *ACS Catal.* **2018**, *8*, 1338−1345.
(58) Wang, Z.; Danovich, D.; Ramanan, R.; Shaik, S. Oriented-External Electric Fields Create Absolute Enantioselectivity in Diels-

https://doi.org/10.1021/acs.inorgchem.2c04119
Inorg. Chem. 2023, 62, 2342−2358

Alder Reactions: Importance of the Molecular Dipole Moment. *J. Am. Chem. Soc.* **2018**, *140*, 13350−13359.
(59) Harvey, J. N.; Aschi, M.; Schwarz, H.; Koch, W. The singlet and triplet states of phenyl cation. A hybrid approach for locating minimum energy crossing points between non-interacting potential energy surfaces. *Theor. Chem. Acc.* **1998**, *99*, 95−99.
(60) Poli, R.; Harvey, J. N. Spin forbidden chemical reactions of transition metal compounds. New ideas and new computational challenges. *Chem. Soc. Rev.* **2003**, *32*, 1−8.
(61) Sen, A.; Vyas, N.; Pandey, B.; Rajaraman, G. Deciphering the mechanism of oxygen atom transfer by non-heme MnIV-oxo species: anab initioand DFT exploration. *Dalton Trans.* **2020**, *49*, 10380−10393.
(62) Rajaraman, G.; Sen, A.; Swain, A.; Pandey, B.; Ansari, A.Identical Spin Multi-State Reactivity Towards C-H Bond Activation in High-valent Fe/Mn-Oxo/Hydroxo Species. **2022**, ChemRxiv:2022-2sqgf.
(63) Sen, A.; Rajaraman, G. Can you break the oxo-wall? A multiconfigurational perspective. *Faraday Discuss.* **2022**, *234*, 175−194.
(64) Kozuch, S.; Martin, J. M. "Turning Over" Definitions in Catalytic Cycles. *ACS Catal.* **2012**, *2*, 2787−2794.
(65) Kozuch, S.; Shaik, S. How to conceptualize catalytic cycles? The energetic span model. *Acc. Chem. Res.* **2011**, *44*, 101−110.
(66) Badiei, Y. M.; Wang, W.-H.; Hull, J. F.; Szalda, D. J.; Muckerman, J. T.; Himeda, Y.; Fujita, E. Cp*Co(III) Catalysts with Proton-Responsive Ligands for Carbon Dioxide Hydrogenation in Aqueous Media. *Inorg. Chem.* **2013**, *52*, 12576−12586.
(67) Jeletic, M. S.; Mock, M. T.; Appel, A. M.; Linehan, J. C. A cobalt-based catalyst for the hydrogenation of CO2 under ambient conditions. *J. Am. Chem. Soc.* **2013**, *135*, 11533−11536.
(68) Spentzos, A. Z.; Barnes, C. L.; Bernskoetter, W. H. Effective pincer cobalt precatalysts for lewis acid assisted CO2 hydrogenation. *Inorg. Chem.* **2016**, *55*, 8225−8233.
(69) Langer, R.; Diskin-Posner, Y.; Leitus, G.; Shimon, L. J.; Ben-David, Y.; Milstein, D. Low-Pressure Hydrogenation of Carbon Dioxide Catalyzed by an Iron Pincer Complex Exhibiting Noble Metal Activity. *Angew. Chem.* **2011**, *123*, 10122−10126.
(70) Bertini, F.; Gorgas, N.; Stöger, B.; Peruzzini, M.; Veiros, L. F.; Kirchner, K.; Gonsalvi, L. Efficient and Mild Carbon Dioxide Hydrogenation to Formate Catalyzed by Fe(II) Hydrido Carbonyl Complexes Bearing 2,6-(Diaminopyridyl)diphosphine Pincer Ligands. *ACS Catal.* **2016**, *6*, 2889−2893.
(71) Federsel, C.; Boddien, A.; Jackstell, R.; Jennerjahn, R.; Dyson, P. J.; Scopelliti, R.; Laurenczy, G.; Beller, M. A Well-Defined Iron Catalyst for the Reduction of Bicarbonates and Carbon Dioxide to Formates, Alkyl Formates, and Formamides. *Angew. Chem., Int. Ed.* **2010**, *49*, 9777−9780.
(72) Ziebart, C.; Federsel, C.; Anbarasan, P.; Jackstell, R.; Baumann, W.; Spannenberg, A.; Beller, M. Well-defined iron catalyst for improved hydrogenation of carbon dioxide and bicarbonate. *J. Am. Chem. Soc.* **2012**, *134*, 20701−20704.
(73) Rivada-Wheelaghan, O.; Dauth, A.; Leitus, G.; Diskin-Posner, Y.; Milstein, D. Synthesis and reactivity of iron complexes with a new pyrazine-based pincer ligand, and application in catalytic low-pressure hydrogenation of carbon dioxide. *Inorg. Chem.* **2015**, *54*, 4526−4538.
(74) Fu, S.; Chen, N.-Y.; Liu, X.; Shao, Z.; Luo, S.-P.; Liu, Q. Ligand-Controlled Cobalt-Catalyzed Transfer Hydrogenation of Alkynes: Stereodivergent Synthesis of Z- and E-Alkenes. *J. Am. Chem. Soc.* **2016**, *138*, 8588−8594.

NOTE ADDED AFTER ASAP PUBLICATION

This paper was posted ASAP on January 23, 2023 with incorrect information in the Supporting Information file. The corrected version was reposted on February 6, 2023.

https://doi.org/10.1021/acs.inorgchem.2c04119
Inorg. Chem. 2023, 62, 2342−2358